ALP-1997-102

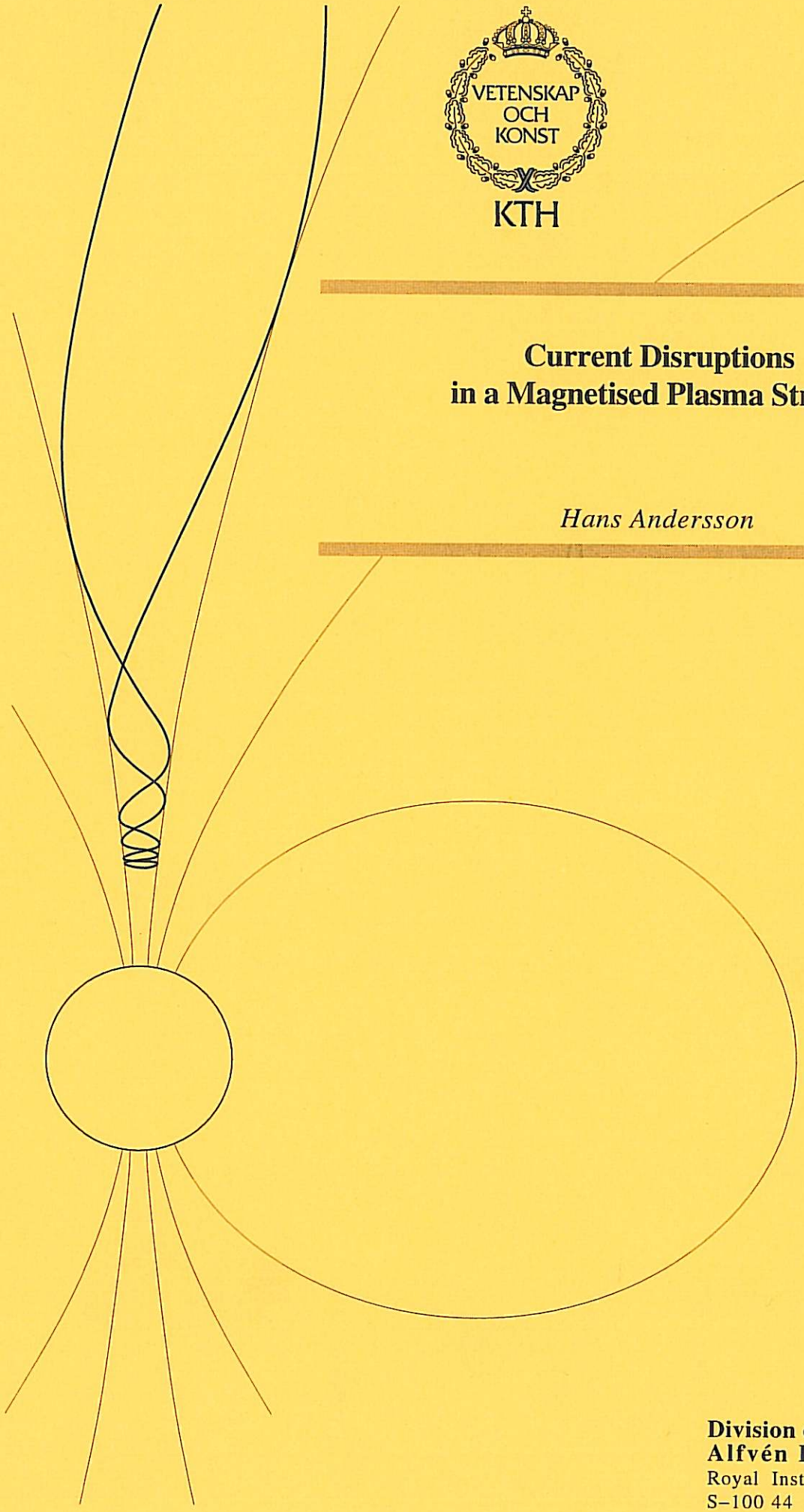

Current Disruptions in a Magnetised Plasma Stream

Hans Andersson

Division of Plasma Physics
Alfvén Laboratory
Royal Institute of Technology
S–100 44 Stockholm, Sweden

Current Disruptions in a Magnetised Plasma Stream

Hans Andersson

Examensarbete
Avdelningen för Plasmafysik
Alfvénlaboratoriet
Kungl. Tekniska Högskolan
Stockholm

mars 1997

Abstract

Measurements are performed to investigate the current system, during a current disruptions in a plasma driven probe circuit. These consist of potential measurements and density measurements in the vicinity of the ion collecting probe. Preliminary measurements with a Rogowski coil, of the currents within the plasma are performed. Some modifications in the construction of the Rogowski coil in order to suppress oscillations and enhance high frequency performance are made. To obtain a fast and accurate positioning of the probes, a program is made for a computer controlled and motorised probe positioning system.

Contents

1 Introduction

When two externally connected probes are placed in a plasma and are differentially separated in potential from the local plasma potential, a current is drawn between the probes. With a sufficiently high bias in a flowing plasma, the current between the probes sometimes starts to disrupt repeatedly. The current generally disrupts from a level below the electron saturation current, and drops to a level close to the ion saturation current (Svensson, 96).

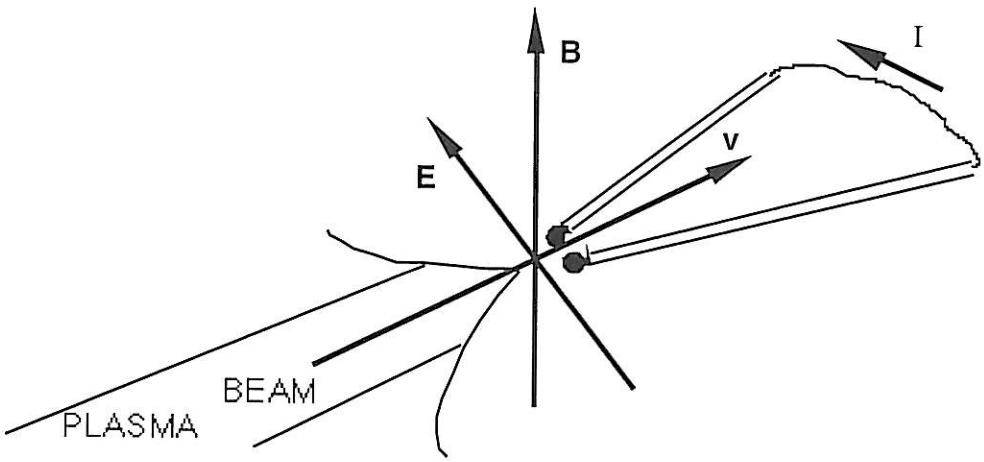

Fig. 1 An electric field is induced by **-v x B** and a current flows between the probes since the probe in the higher potential repels the electrons.

The phenomenon was discovered in 1976, with probes only biased by the electric field produced by the plasma moving perpendicular to a magnetic field. The apparently instant drop of the current could not be further investigated at that time since the time resolution for oscilloscopes available was not sufficient.

In 1996 a project started, for the study of the current disruptions. An important parameter involved is the density of the plasma. To provide an accurate local measurement of the density, Romedahl (1996) calibrated a density probe against an interferometer. Consecutive measurements with a density probe, stepping across the beam, was integrated and compared with the well documented accuracy of the interferometer. The probes shows a density twice the density measured with an interferometer.

Svensson (1996) found that the disruptions is a general behaviour and not dependent on the way they are biased or the shapes of the probes. He also proved that the disruption originates at, or very close to the ion collecting probe, and presented a cathode spot theory for a possible electron emission at the ion collecting probe, necessary to maintain the currents above the ion saturation level. Also he noted that the drop in the current is accompanied by a drop in the potential of the probe system. The time for the current to drop can vary, times from 10 ns to 105 ns has been observed (Svensson, 96). The short times are for a double probe, where the leads are placed in the same shaft, minimising the inductance, and the long times are for probes connected with an inductance of 50 μH added in the external circuit.

The aim of this work is to investigate further the interaction between disruptions and plasma parameters, and map the propagation of currents in the plasma.

2 Apparatus

2.1 The plasma source

The device used is a plasma gun with a conical theta pinch producing a fast flowing plasma beam that travels along a longitudinal magnetic field before it enters the interaction space, with a transverse magnetic field inducing the electric field necessary for this experiment, $\mathbf{E}=-\mathbf{v} \times \mathbf{B}$.

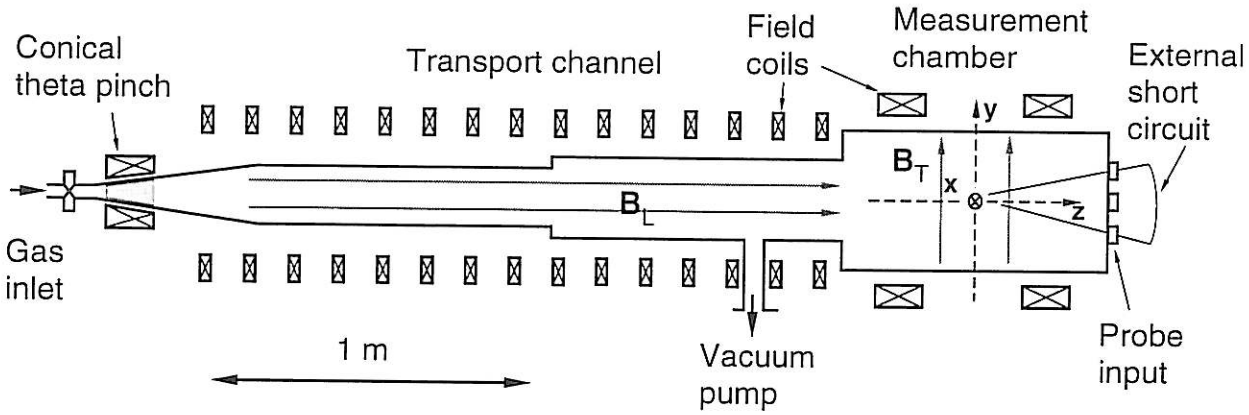

Fig 2 A cross section of the plasma gun (Svensson, 96).

The plasma is formed in a conical theta pinch, which consist of a glass cone, and a one turn coil placed around the glass cone. The glass cone is open in both ends to allow a small amount of hydrogen gas to enter in one end of the cone and after ionisation leave the cone as plasma, out of the other.

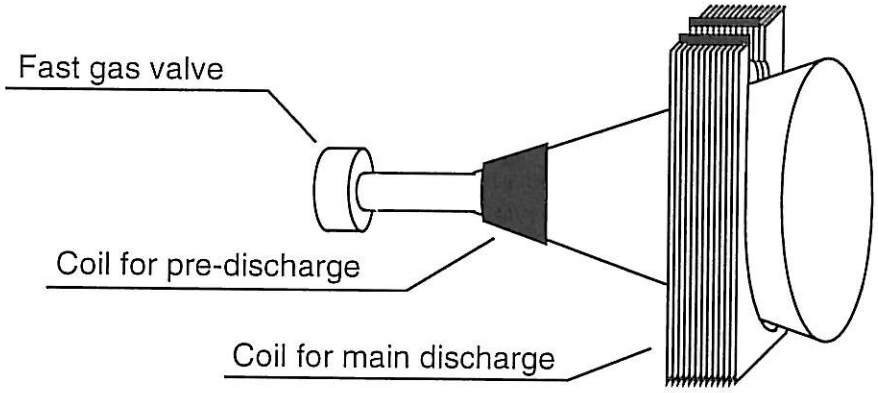

Fig. 3 The conical θ-pinch

The gas valve opens after 3.3 ms in the first half period of oscillation of the current in the magnetic coils of the longitudinal and transverse magnetic fields of the gun, and hydrogen gas of 665 mm Hg is let in for typically 170 μs. A shorter opening time results in a less dense plasma, and a longer opening time, allows neutral gas particles to migrate beyond the fringe of ionisation in the cone, causing a disturbed and slower plasma. Then the plasma is pre-ionised by a 32 kV discharge of a small capacitor bank, over a spark gap that produces a 3 MHz current in a flat single loop around the θ-pinch.

After 3 μs the main ionisation takes place. A big capacitor bank is discharged over a spark gap and a damped 300 kHz sinusoidal current oscillating in the main coil, induces an azimuthal field in the cone, and by the force of **j** x **B** the partly ionised plasma is concentrated to the axis of symmetry where it is further ionised by collisions. The plasma is squeezed out of the cone, and the forward direction is given by the geometry (Fälthammar, 91). the plasma then propagates through a region of a longitudinal magnetic field of 0.1 T. The diameter of the tube is then increased and the magnetic field is gradually expanded. The plasma beam enters the interaction chamber 2.7 meters from the source at a velocity varying from 300 km/s for the first arriving particles down to 100 km/s for the late arriving particles. A transverse magnetic field of 0.02 T in the upward direction is producing an electric field across the interaction chamber, according to **E**=-**v** x **B** . This electric field lasts for 20 μs which is the duration of the plasma pulse.

Magnetic field	B_T	0.02 T
Density	n_e	10^{19} m^{-3} *
Electron temperature	T_e	5-10 eV *
Debye lenght	λ_D	10^{-5} m
Plasma translational velocity	v	250 km/s
Electron thermal velocity	v_e	1800 km/s
Ion gyro radius at translational velocity	r_{gi}	100 mm
Electron gyro radius	r_{ge}	0.5 mm
Ion gyro frequency	f_{gi}	300 kHz
Electron gyro frequency	f_{ge}	560 MHz
Lower hybrid frequency	f_{lh}	13 MHz
Electron plasma frequency	f_{pe}	30 GHz
Group velocity for a 40 MHz whistler wave	v_w	3000 km/s

* An approximation based on earlier measured values for similar settings of the gun.

Table 1 Plasma parameters in the interaction space.

The plasma is practically collision less. The ions have translational velocities several times their thermal velocities, but for the electrons the thermal velocities and the translational velocities are in a reciprocal relation. For simplicity the ions are said to move along the Z-axis, and the electrons along the Y-axis trapped by the magnetic field lines.

2.2 Probes

The disruption probes

The disruption probes consist of a copper sphere mounted on a glass shaft, and are used in pairs connected externally. This arrangement makes the two spheres become equal in potential, except during rapid changes in the current, when the inductance in the circuit must be considered. The sphere positioned in the higher potential is repelling electrons because of the external connection to the lower potential, and is therefore called the ion collecting probe or ICP. The sphere positioned in the lower potential is attracting electrons because of the external connection and is called the electron collecting probe or ECP in analogy.

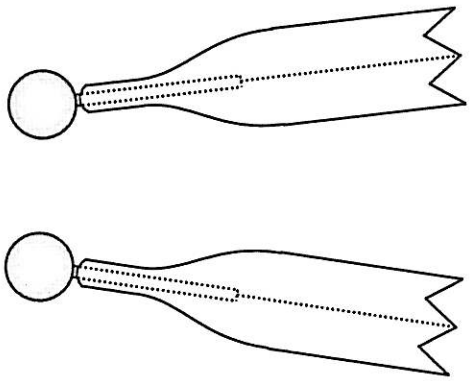

Fig 4
The disruption probes
in scale 2:1
(Svensson, 96).

The Pearson current probe

For the measurements of the current in the external connection between the disruption probes a current monitor model 2877 from Pearson Electronics is used, with the maximum specification of 100 A and 200 MHz. It has a voltage response of 1 V/A.

The potential probes

For the potential measurements, the electric field probe included in a combined density probe and electric field probe (Brenning, Lindberg and Eriksson, 81). has been used. (See **Fig. 5a**).

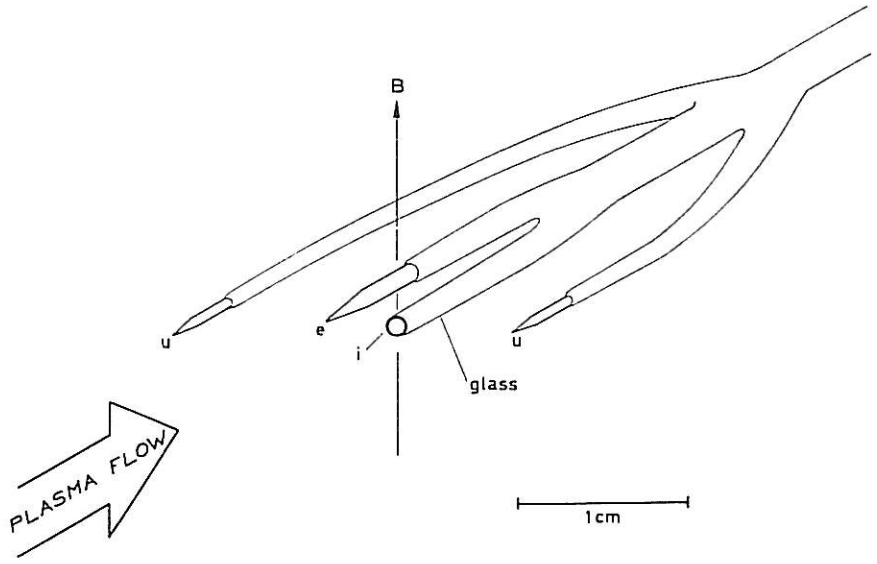

Fig. 5 a The combined probe (Brenning, Lindberg and Eriksson, 81), used for the potential and density measurements.

The Density probe

The density probe used in these measurements is the combined density probe and electric field probe (Brenning, Lindberg and Eriksson, 81). The density probe consists of a cathode with a small circular surface facing the direction of the source of the plasma, and an anode shaped as a pointed needle. The probe is externally biased with 25 V to repel the electrons from the cathode, and the anode has a sufficiently large area to maintain the necessary electron current, to match the ion flux at the cathode. The probe is measuring the incoming flux of ions to the small surface and is therefore directional sensitive. Since the output current is proportional to the incoming ion flux, the velocity of the plasma is needed for the the calculation. The density is obtained from the equation $n_e=I/(v_{pl}\cdot e\cdot A)$. An advantage is that it provides a local measurement of the density.

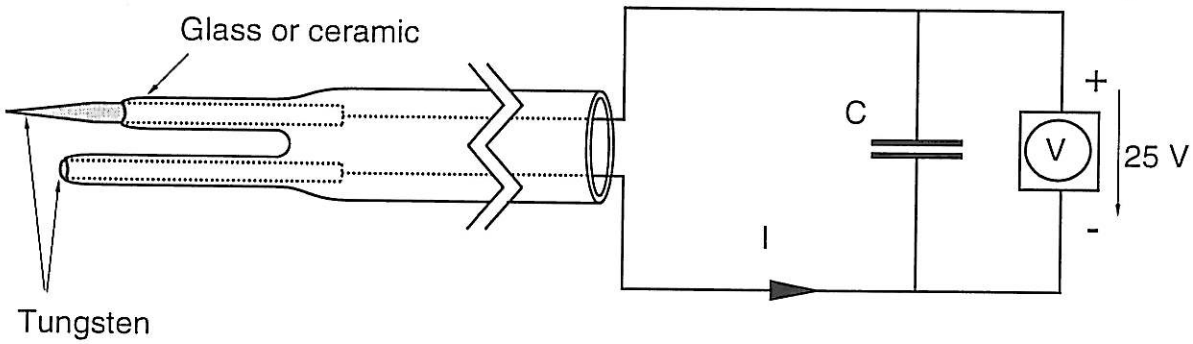

Fig. 5b The density measuring part of the combined probe (Svensson, 96).

The magnetic coil

The induced voltage in a magnetic coil is proportional to the rate of change in the magnetic flux through the coil

$$V=\frac{dB}{dt} N A \qquad \textbf{(Eq. 1)}$$

were N is the number of loops in the coil and A is the bounded area perpendicular to the magnetic flux.The number of loops in the coil can vary, from one for a single loop to a thousand for a Rogowski coil.

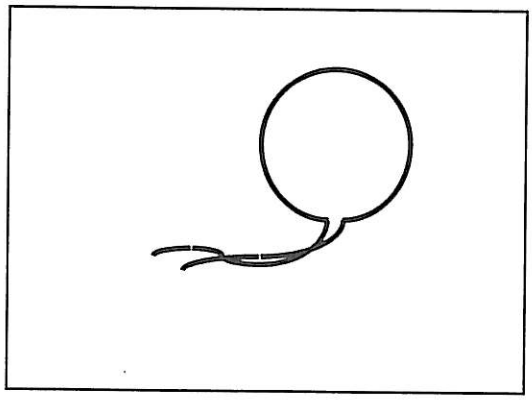

Fig. 6
The simplest form of a magnetic coil is a single loop of wire.

The Rogowski coil

In the case of the Rogowski coil the length of the coil is used to make an almost closed loop around a current.This construction makes the voltage from the coil proportional to the rate of change in the current (Hutchinson, 87). The current is obtained by integration of the signal. This integration is normally made with an RC-circuit at the input of the oscilloscope.

In order to calculate the induced voltage in a Rogowski coil for a certain current derivative, Ampere's law of circulation and the integral form of Faraday's law, may be written as (Hutchinson, 87),

$$v_i = -\frac{d\Phi}{dt} = -\oint \frac{d}{dt}(anBds) = -\mu_0 an\frac{dI}{dt} \qquad \textbf{(Eq. 2)}$$

where v_i is the induced voltage, a is the cross section area in mm of the turns in the coil, n is the number of turns per mm and I is the net current through the loop. By insertion of a and n the induced voltage in the Rogowski coil for a certain rate of change in the current is obtained.

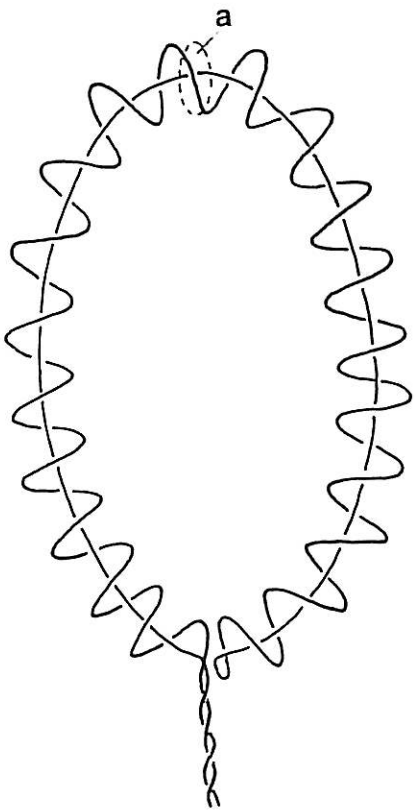

Fig. 7 A schematic view of a Rogowski coil (Hutchinson, 87).

To obtain the current from the derivative of the current, the signal from the Rogowski coil is integrated. For an analogue integrating RC-circuit the output voltage is obtained by

$$v_{out} = \frac{1}{R\,C}\int_0^t v_i\,dt \qquad \textbf{(Eq. 3)}$$

provided that $t << R{\cdot}C$.

In the case of LR-integrating circuit the voltage over the resistor is

$$v_{out} = \frac{R}{L}\int_0^t v_i\,dt \qquad \textbf{(Eq. 4)}$$

provided that $t << L/R$.

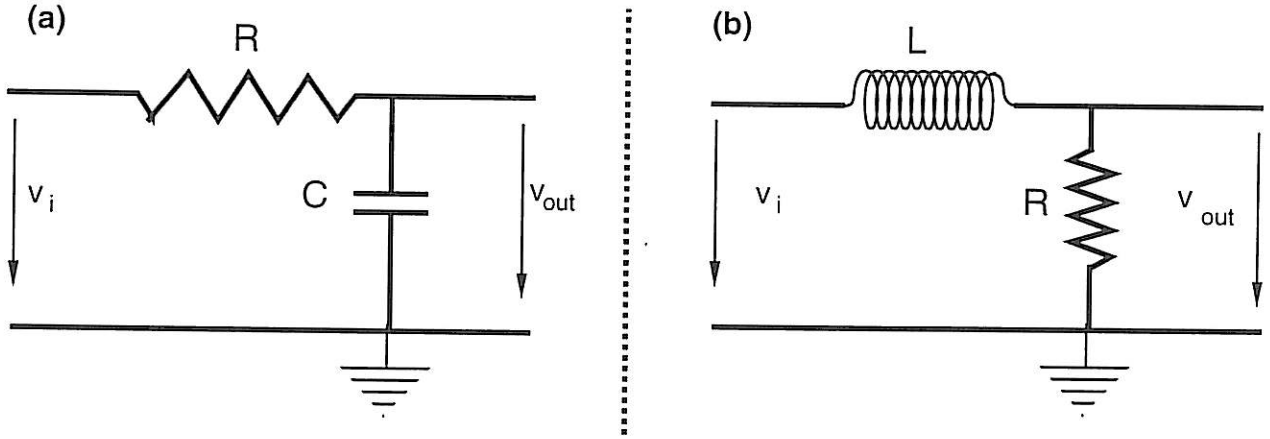

Fig. 8 Two examples of integrating circuits. (a) RC-circuit and (b) LR-circuit.

Three existing Rogowski coils were tested against the Pearson current probe, to evaluate their operation at the high frequency regime corresponding to the time derivatives of the current in a disruption. One probe with the Rogowski coil in a plane perpendicular to the probe shaft referred to as the 90° probe, and two probes with the loop of the Rogowski coil aligned with the probe shaft. These two probes are identical except for the colours and referred to as the red probe and the black probe. Preliminary tests indicated that there are some advantages in suppression of resonance oscillations, if the inductance of the Rogowski coil itself is used for the integration, as in a LR-integrator shown in **Fig. 8b**.

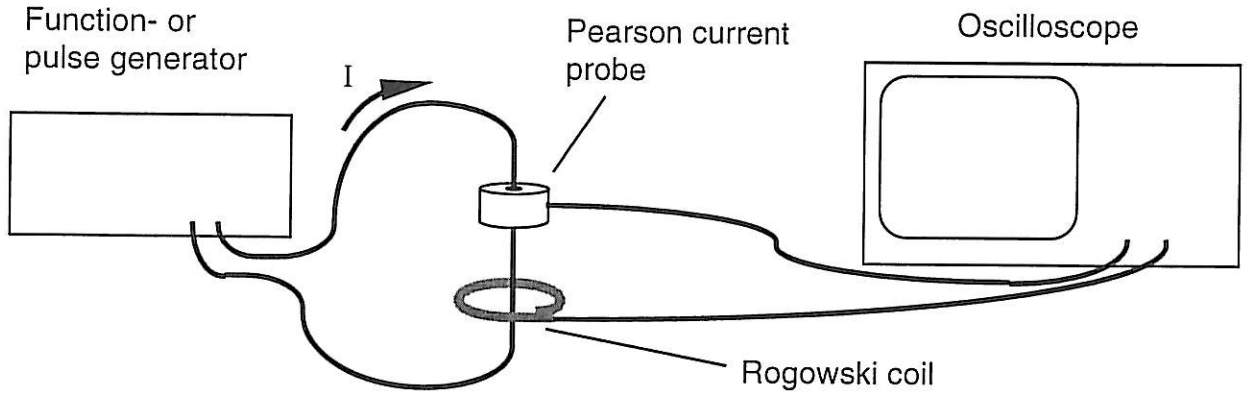

Fig. 9 Circuit for test of Rogowski coils against the Pearson current probe.

The signal from a function generator was led through the coils and the current probe and the voltages induced were measured over a 50 ohm termination, with an oscilloscope and saved.The probes were first tested with a 2 MHz sawtooth wave.The derivatives of the current was 95 kA/s for the positive slope and -1.23 MA/s for the negative slope.

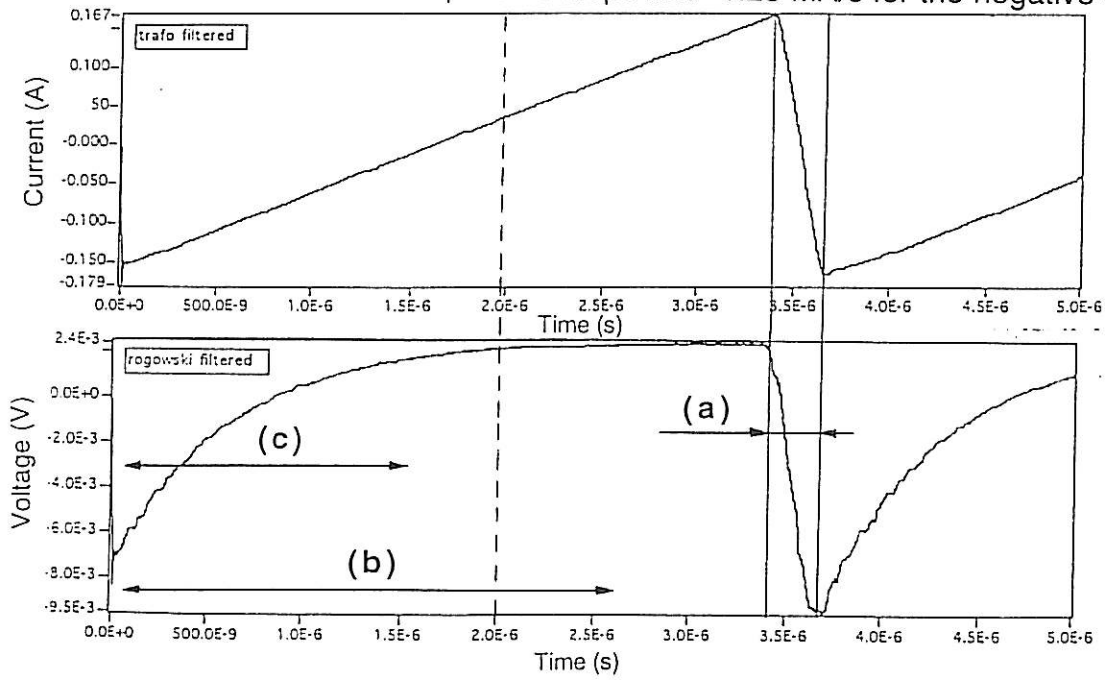

Fig 10 The output voltage from the "Red" Rogowski coil for two different derivative of the current measured with the Pearson current probe. It seems that the fast decrease of the negative slope **(a)** satisfies t << R/L, **(t < 20 ns)** while the slower rise **(b)** does not. After 2 μs the probe measures the derivative **(t > 2 μs)**. For times **(20 ns < t < 2 μs) (c)**, the signal is a mix of the derivative and the current, the interpretation is uncertain.

Resonances

At high derivatives of the current through the coil the signal from the coil starts to oscillate. The big 90° Rogowski coil shows pronounced oscillations. When the cable carrying the signal from the function generator was moved around inside the Rogowski coil the amplitude of the oscillations changed. When the current carrying cable is positioned with equal lengths of the coil on each side, the oscillations are minimised (See **Fig. 11**).

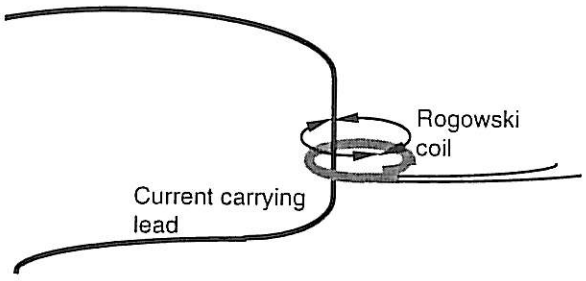

Fig. 11 The position of the current in the coil, for minimising the oscillations.

These oscillations are interpreted as resonances in the circuit consisting of the distributed capacitances and inductances in the Rogowski coil, and the electrostatic shield around the coil. This is picked up by the oscilloscope as illustrated in **Fig. 12.** Since the derivative of the resonance is of the same magnitude as the disruptions they can not easily be filtered out.

On the Rogowski coils tested, the shielding is connected to the instrument ground and to one end of the coil. An induced capacitive current between the shield and the coil can close in in a loop in point A, or over the termination resistor in B, where it will mix with the signal measured by the oscilloscope.

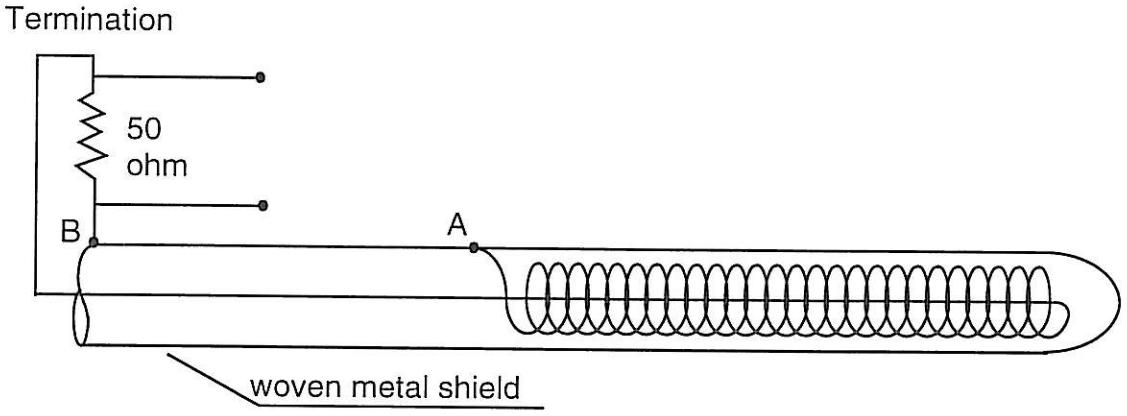

Fig. 12 A schematic view of the shield construction of the tested probes. The coil is drawn straightened out for clarity.

To reduce the oscillations a Rogowski coil with very few turns were made. This coil has about 0.5 turns/mm and a cross section of the turns of approximately 6 mm^2. To minimise the effect of currents in the shield this Rogowski coil has an additional shield connected to the ground of the oscilloscope. With these improvements the resonance oscillations were suppressed, or did not mix with the measured signal. Preliminary tests indicated that there are some advantages in suppression of the resonance oscillation, if the inductance of the Rogowski coil itself is used for the integration, as in a LR-integrator. Since the inductance is not well defined however, the Rogowski coil is calibrated against the current probe for currents in the external connection of the disruption probes (described in section **3.2**).

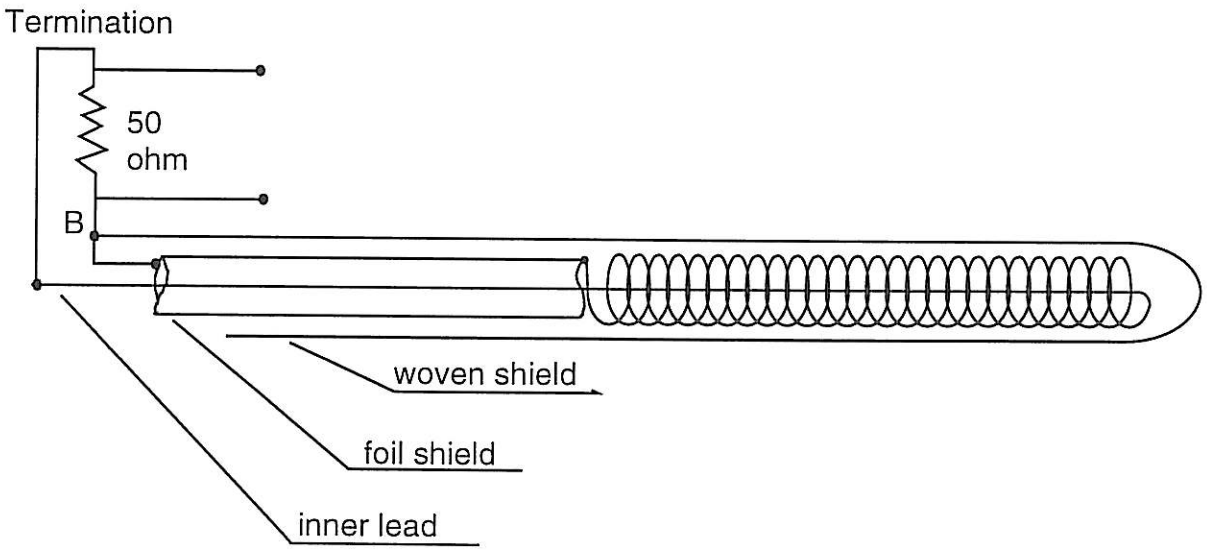

Fig. 13 A schematic view of the shield construction of the improved Rogowski coil. The coil is drawn straightened out for clarity.

2.3 Data acquisition

Computer

A LabVIEW program, run on a Macintosh personal computer was used to control and to save the sampled sequences from the oscilloscope. Integration of the signal from the Rogowski coils and some filtering, was all made in LabVIEW. It was also used for the positioning of some probes in combination with a probe guidance system.

Oscilloscope

All measurements were performed using a Tektronix 684A digitising oscilloscope with a maximum sampling rate of 5 GHz.

The probe guidance system

To allow a probe to be positioned at an arbitrary point in space, a probe guidance system was developed with three degrees of freedom. The construction is developed on a existing system with rotation, and translation in the direction of the probe shaft, with two additional features, the ability of rotation around the X- and Y-axis. The rotational movement is not used in the program written for the positioning, but could easily be added if necessary, and is useful for manual adjustments. The guidance system provides, besides the positioning of the probe mounted, a fast and accurate way of placing stationary probes at desired positions, by using the mounted probe as a reference. Four small DC motors supported by computer controlled power supplies, does the work of moving the probe around. The motors has a system of proximity switches and as feedback, a DC voltage proportional to the position. The output voltage can be adjusted to achieve a smooth movement, on the power supplies, where also further limitations of the maximum ranges within which the probe is allowed to be moved, can be set. The direction and the on/off function is set at an input of the power supplies, and the feed back voltage from the motors can be measured at the outputs. The computer controlled switch is a HP3488A, and is controlled by LabVIEW and a GPIB card. Besides the directional and and on/off switching of the power supplies, the HP3488A is also used as a multiplexer to switch between the different motors when measuring the positions. This way only one GPIB controlled multi meter is required.

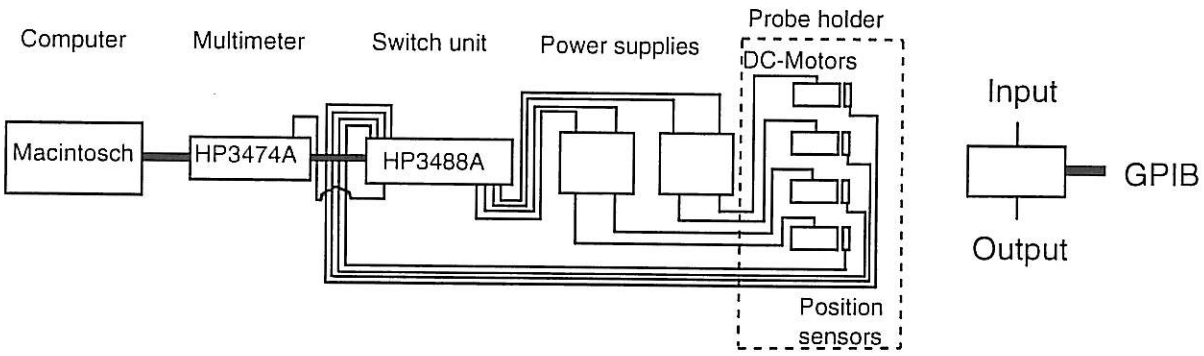

Fig. 15 A schematic overview of the guidance system. The lines in the figure does not represent individual leads.

A controller program called "Probe mover X, Y and Z" is written to step through a volume and perform a measurement for each position stepped through. The number of steps in each direction are set at the panel, likewise are the coordinates that are limiting the volume. It is advisable to fill in the total delay (from shot, to sweep start of the oscilloscope) on the panel (**Fig. 16**) since this value is available to the acquisition program together with the coordinates. The length, from the measuring point of the probe, to the centre of rotation, is needed for calculation of the translational movement required to get to the position. The translational movement is preceded by rotations around the Y and X axis.

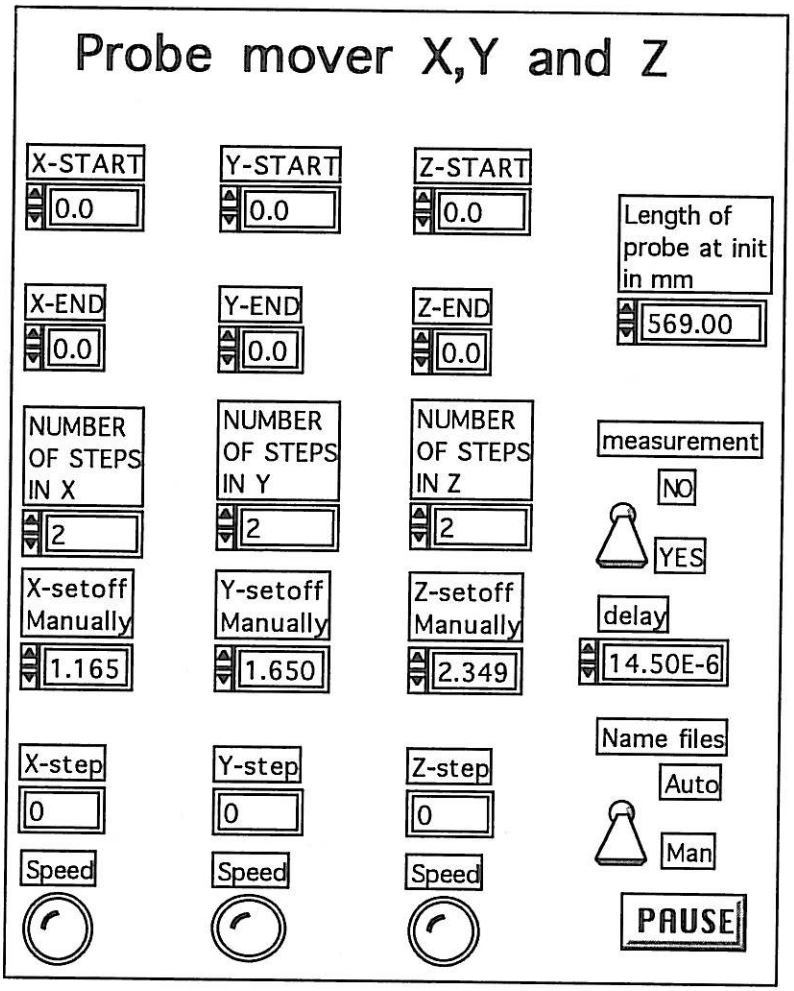

Fig. 16 The panel is the user interface of the LabVIEW program. See **appendix A** for explanations.

If a surface is to be stepped through rather than a volume, the X-Y plane is obtained by interrupting the program after the first "slice" since this is the order the program steps through the volume. For the X-Z plane and the Y-Z plane, minor changes of the diagram have to be made. The formula window for calculation of movement along the excluded axis is edited, and the "for" value of "steps" in the for loop of the excluded axis is set to 1 instead. This can not be made by setting "steps" to 1 on the panel since this causes division by zero in a formula. In the formula window of the diagram in **Fig. 17**, the changes are made for the X-Z plane.

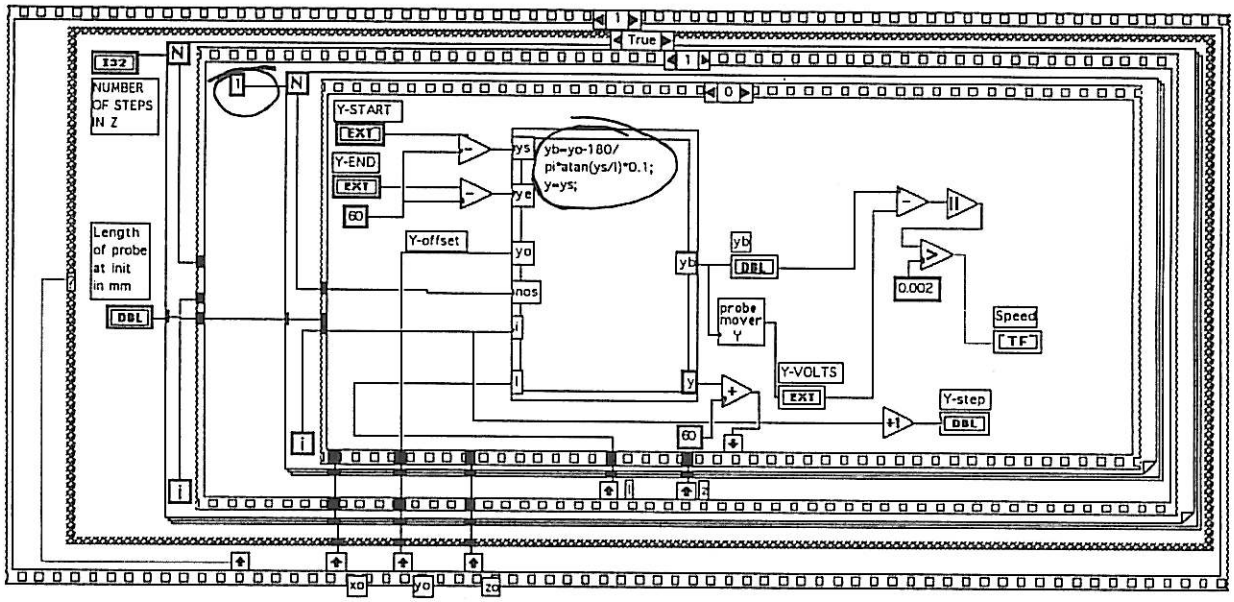

Fig. 17 The diagram which is the programming interface of the LabVIEW program.

This is the order of actions in the program, starting with rotation about the Y axis

1 The angular value is calculated and converted to a voltage.

2 The direction is decided from the present voltage and consecutive measurements during the movement checks if the values are close enough.

3 When it is, the power is shut of and the same procedure is performed for rotation about the X axis.

4 At this stage the probe is pointing in the correct direction and a final translational movement is made in the same manner.

5 The program calls a sub routine for acquisition of the data.

6 When the preceding steps have been performed for all points in the volume, the probe is repositioned and the program is ended.

3 Measurements

The aim of these measurements is to go a step further compared to the earlier work which focused on the disruptions' origin of location, and the mechanism of feeding of the high currents involved. Here we will focus on the disruptions interaction with the plasma, with current and potential measurements in the plasma. One issue of interest is how the current system through the external loop closes within the plasma. Another question is if it is possible see a correlation between the rapid probe potential variations in the disruption and a variation in the plasma potential.

3.1 Expected current system

In a series of experiments performed by R. L. Stenzel and J. M. Urrutia at the Department of Physics, University of California, Los Angeles, current distribution in space and time of pulsed currents in tethered electrodes was studied.They have also shown the formation of whistler wings, by simulation of relative motion of the magnetic field and the electrodes, by superimposing the effects of adjacent current pulses. Their experiments are conducted in a large afterglow plasma, with two externally biased electrodes.

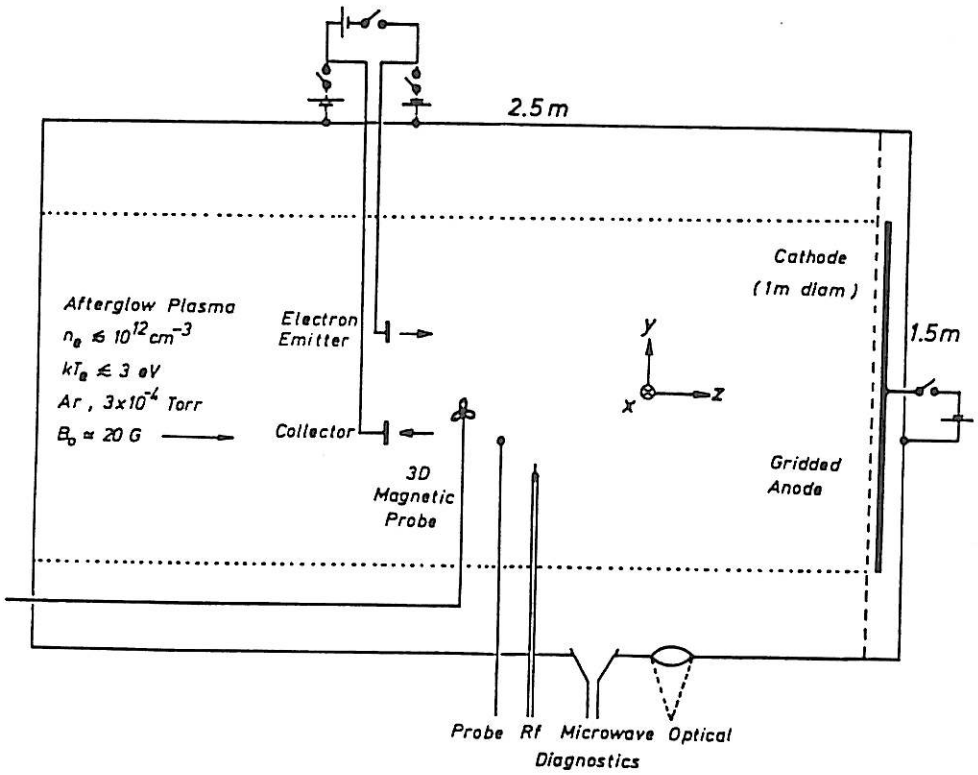

Fig. 18 Schematic arrangement of the plasma device. (Stenzel and Urrutia, 90).

In the case of a uniformly moving current-carrying electrode, the time the electrode stays on a field line is experienced by the plasma as a current pulse on that particular field line, with a pulse length decided by the velocity and size of the electrode. A variable transformation to the rest frame of the electrode does not change the physics.

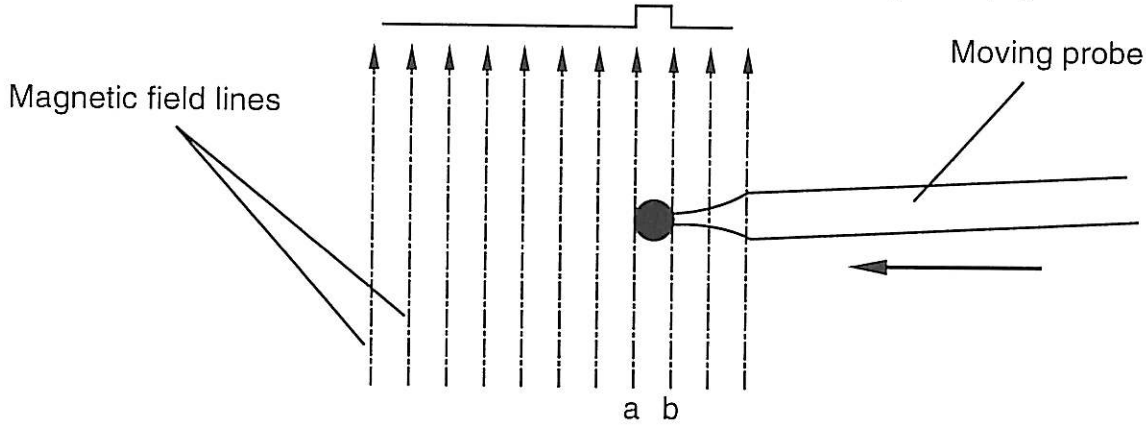

Fig. 19 The magnetic field line **(a)** is about to come in contact with the electrode and the magnetic field line **(b)** is left by the electrode.

Stenzel and Urrutia have developed a method for simulation of tethered electrodes, moving relative to the magnetic field. They apply small amplitude current pulses of the order of ion saturation current to the electrodes. Currents of such a low amplitude do not give rise to nonlinearities, instabilities or plasma modifications. By superimposing the magnetic fields from pulses, with delays increasing in steps of the pulse length, they simulate a moving electrode. The result after superimposing several pulses is the magnetic field in the plasma, as if a DC current was drawn between the electrodes, moving across the magnetic field. (See **Fig. 20**)

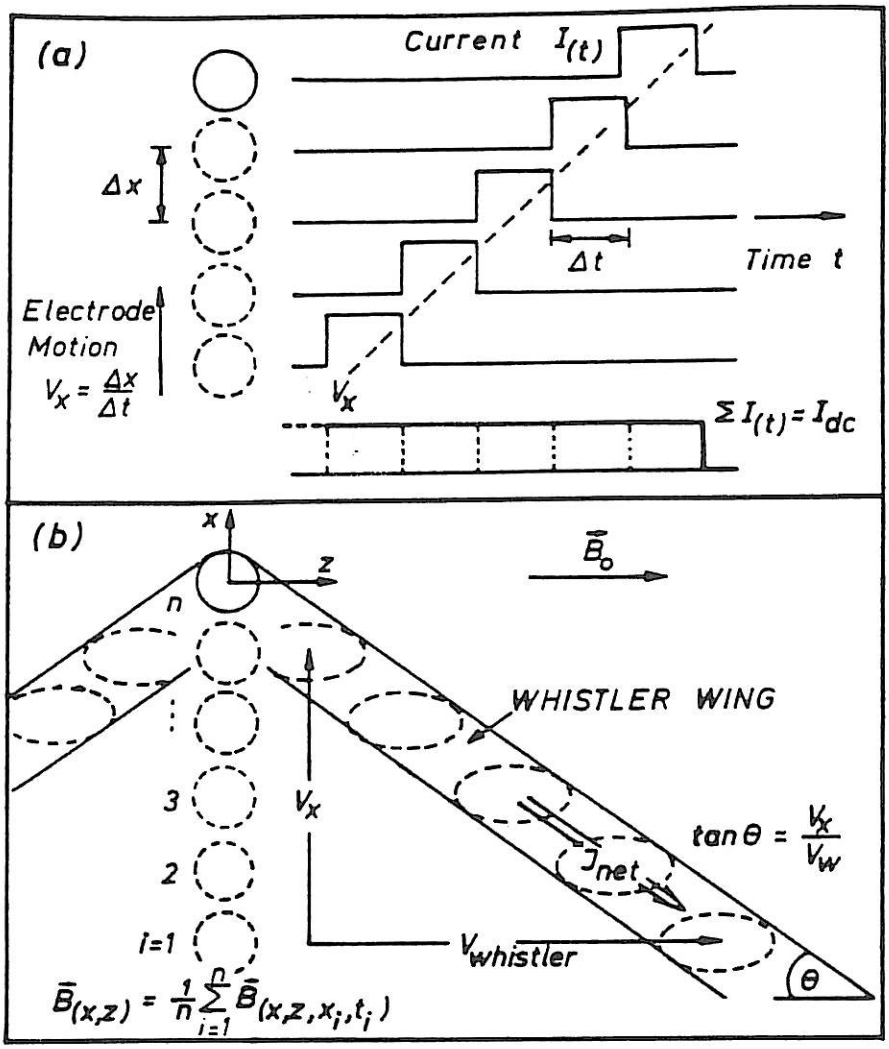

Fig. 20 Schematic diagram demonstrating the measurement method for obtaining currents from moving electrodes. **(a)** The continuous motion of an electrode is replaced by a sequence of displacements Δx while the continuous current I_{dc} is broken up into a sequence of pulses delayed by Δt consistent with the velocity $v = \Delta x/\Delta t$. **(b)** As the electrode moves with velocity v_x across $\mathbf{B}_0$, it emits at each position a current pulse which propagates along $\mathbf{B}_0$ at the whistler wave speed. The superposition of all pulses yields a wing like pattern at a Cherenkov-type angle $\theta = \tan^{-1}(v_x / v_w)$. In the experiment, the field distributions $\mathbf{B}_i$ (x,z) are recorded from separate shots for i=1...20 different electrode positions and subsequently superimposed (Figure and caption text from Stenzel and Urrutia, 90).

The magnetic field in Stenzel and Urrutia's experiment exhibits an oscillatory transient whenever the current of the electrodes is switched on or off. At each fixed position, the frequency of the disturbance of the magnetic field is found to decrease in time, because the propagation speed of the disturbance is decreasing with frequency. At higher electron densities and lower initial magnetic fields the propagation speed decreases, but remains unaffected by changes in the electron temperature. This behaviour shows that the current is carried by a wave, and not by particle migration. A measurement of the wavelengths at different frequencies shows very good agreement with the theoretical dispersion relation for whistlers (Stenzel and Urrutia, 90). From measurements of orthogonal magnetic field components, the wave is found to be right hand polarised according to Stenzel and Urrutia. It has been shown (Stenzel and Urrutia, 90) that wave emission in the bands ($\omega_{lh} < \omega < \Omega_e$) and ($\omega_p < \omega < \omega_{uh}$) can take place, and with appropriate parameters dominate the emission in the Alfvén band ($\omega < \Omega_i$). The conditions for which these observation is expected to hold is, for electrode dimensions smaller than an ion Larmour radius and pulses shorter than an ion cyclotron period.

Our experiment has large similarities with the simulated experiment shown in **Fig. 1 9** of a probe moving relative a plasma, synthesised by Stenzel and Urrutia. In our experiment a DC current between the probes is expected from the electric field $\mathbf{E}=-\mathbf{v} \times \mathbf{B}$, where the velocity is approximately 200 km/s. The probes are biased by an electric field of 5kV/m. With a diameter of 5 mm the plasma experiences pulses of 25 ns duration, obtained from the time required for the plasma to propagate 5 mm. This gives a centre frequency of 40 MHz (Stenzel and Urrutia, 90) of the oscillations exited. The spheres of the ICP and ECP are much smaller than the ion gyro radius (0.1 m) which is one condition required. Other conditions of the experiment performed by Stenzel and Urrutia that justifies the use of the plane wave, infinite medium theory (Stenzel and Urrutia, 90), are also fulfilled in our experiment. The propagation speed of a whistler packet (the group velocity) is given by Stenzel and Urrutia, (90) as

$$v_g = 2\,c\,\sqrt{\frac{\omega\,\Omega_e}{\omega_p^2}} \qquad \textbf{(Eq. 5)}$$

which for our centre frequency of 40 MHz gives v_g=3000 km/s for the parameters of our plasma.

For a plasma velocity of 200 km/s the central axis of the resultant whistler wing deviates $\tan^{-1}(v_g/v_{pl}) = 4°$ from the Y-axis. The sphere of the probe is much smaller than the parallel wavelength of the whistler (0.1 m). In this case the sphere is expected to radiate like a point source, and the current is spread within the whistler ray cone (half angle=19°) (Stenzel and Urrutia, -90). With a probe separation of 20 mm the whistler wings will begin to overlap within 3 cm and possibly define the scale length of beginning current closure.

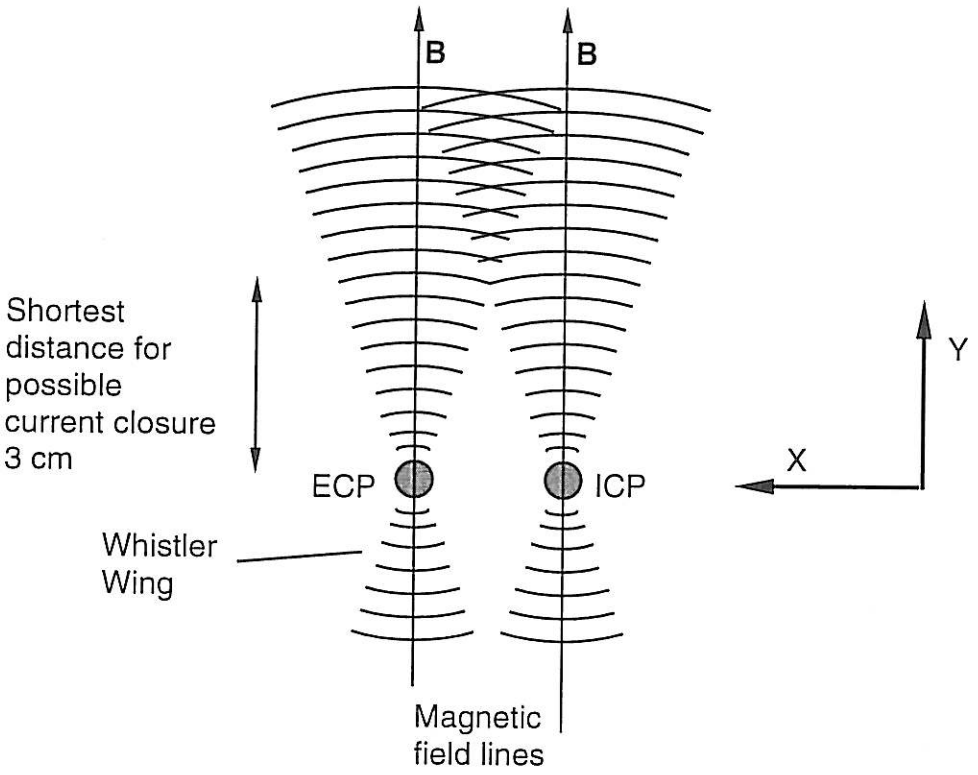

Fig. 21 The whistler wings from the disruption probes, looking along the path of the plasma. The parallel wavelength is not drawn to scale.

The propagation speed of the whistler wave, 3000 km/s, corresponds to a delay of approximately 3 ns from the probe surface to the distance where the measurements are performed, 1 cm from the sphere. Some of the measuring points lie within the expected whistler wing, some do not.

3.2 Current measurements with a Rogowski coil

As discussed at the of section **2.2** the Rogowski coils need to be tested and calibrated in the frequency range were they will be operated. This is achieved by putting the Rogowski coil around the probe shaft of the ICP, outside the plasma gun. The current is also measured with the Pearson current probe. In **Fig. 22** it is seen that, for the first disruption of 1.75 A, the voltage drop of the Rogowski coil is 10 mV. The average of the current drops and the average of the voltage drops are corresponding to a scaling factor of 5.5 mV/A.

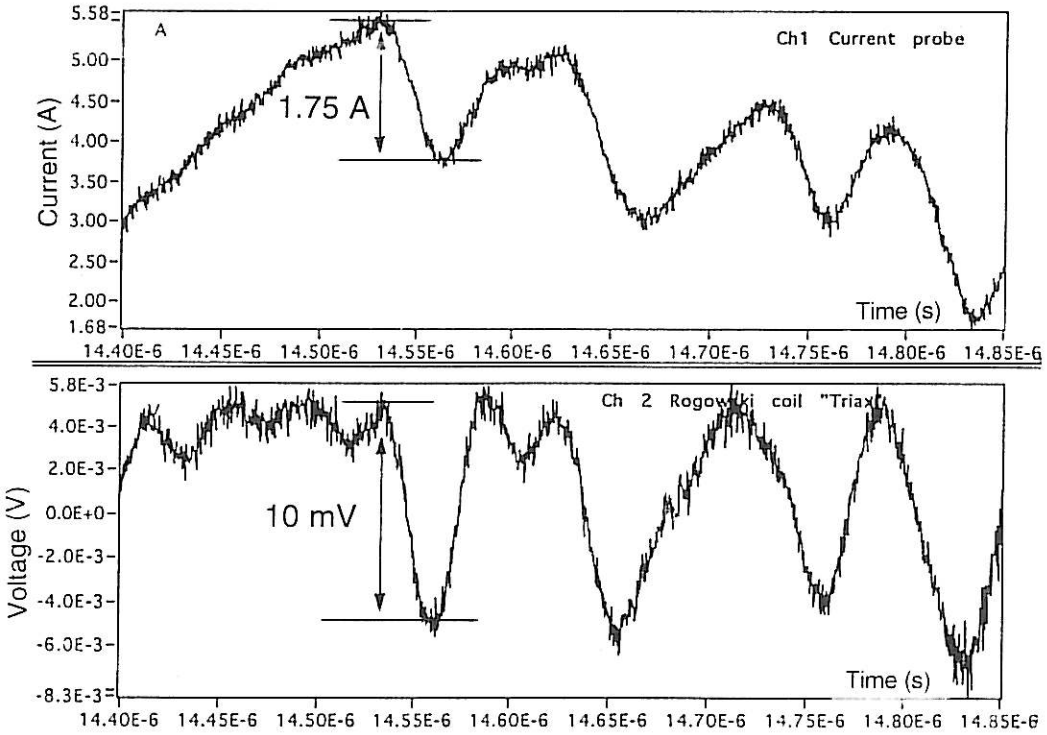

Fig. 22 The signals from the Pearson current probe and a Rogowski coil used as an LR-integrator with R=50Ω. For the short times of a disruption the voltage drop is proportional to the current drop.

There seems to be no problem to resolve the fast disruptions in time with this Rogowski coil, although. Slower variations in the current are filtered out. The next step is to check the signal to noise ratio when the measurement is made inside the plasma gun. The Rogowski coil is placed in an insulated glass tube still with the coil around the ion collecting probe shaft, to be sure to measure the same current as the the Pearson probe does. A result from these measurements is presented below.

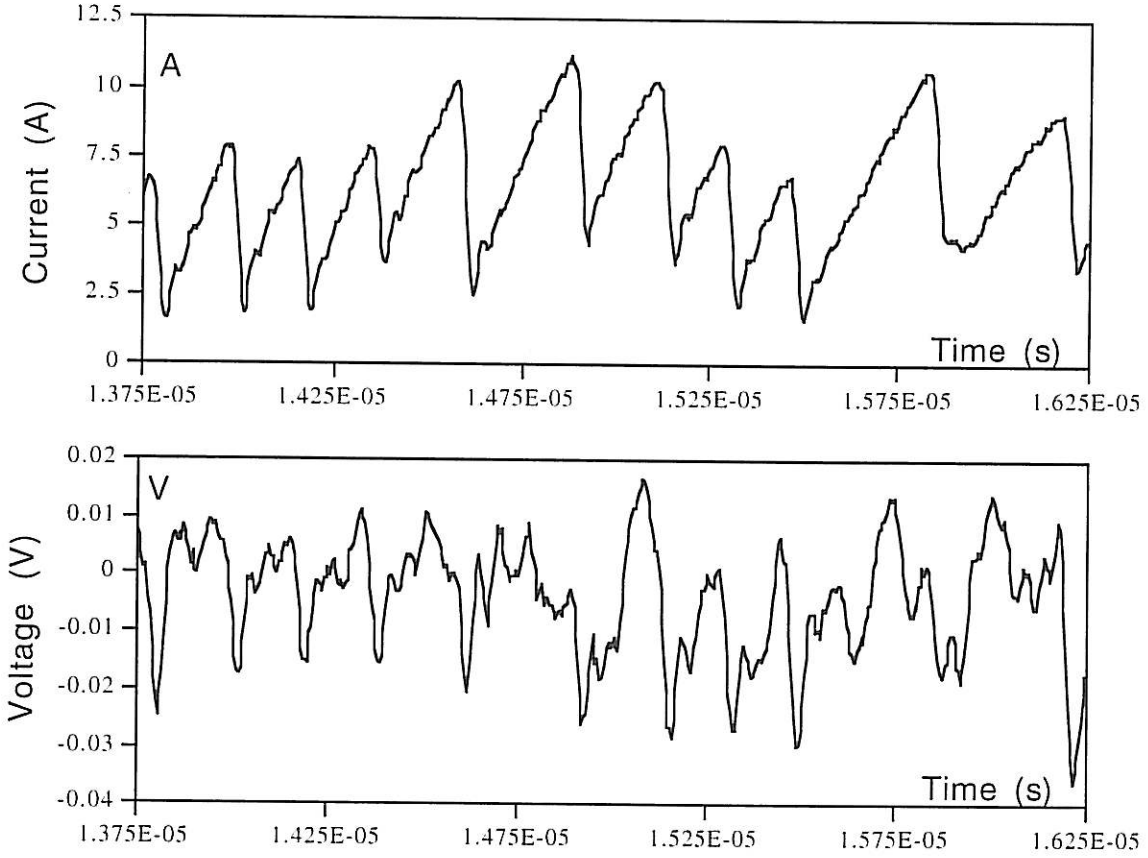

Fig. 23 The signals from the Pearson current probe and a Rogowski coil. The upper curve shows the current measured with the Pearson current probe, and the lower curve shows the voltage from the Rogowski coil with a 50 ohm termination.

When the Rogowski coil is positioned just above the ICP measuring currents perpendicular to the Z-Y-plane, no well defined disruptions have occurred. It is possible that the position of the Rogowski coil is prohibiting the disruptions. There are also, possibly, rapid current variations in the plasma itself. The signal from the Rogowski coil indicates current jumps of 20 A, while the variations measured with the Pearson current probe are within a few Ampere. There is no obvious correlation between the small amplitude variations measured with the current probe and potential jumps of the Rogowski coil. From these few measurements it is not possible to tell if the absence of disruptions is significant for the position of the Rogowski coil.

3.3 Potentials in the plasma without current disruptions

For potential measurements at the disruptions a potential probe is placed below each disruption probe. In this section plasma oscillations at these positions in the absence of disruptions, are investigated. The potential probes are positioned in such a way that the main part of the needles are placed within the same flux tube as the spheres.

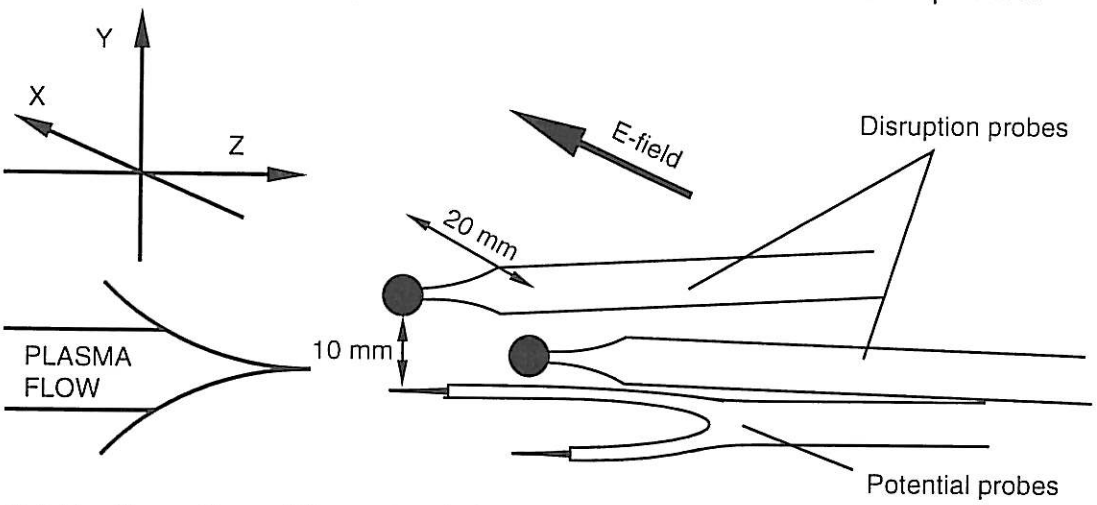

Fig. 24 Configuration of the potential probes. The coordinates (x, y, z) of the spheres of the disruption probes are (-0.02, 0, 0) and (0, 0, 0) respectively.

Common mode oscillations

The potential fluctuations of the plasma beam shown by the dotted and the thin solid line in **Fig. 25** is of the order of 100 to 150 volt, and have estimated typical frequencies of 2-10 MHz. There is almost no difference from shot to shot in terms of amplitude and frequency. The level of the potentials relative to the ground can vary 200 V from shot to shot, but the dominating variations in potential is common to both probes. Those common mode fluctuations are for a probe distance of 20 mm, five times the differential fluctuations, the thick solid line in **Fig. 25**. It is also seen that the common mode fluctuations are gradually decreasing in amplitude towards the end of the pulse. This general potential fluctuation makes it impossible to interpret potentials in the plasma with reference to ground. Instead differential measurements of the two probes are made. Such a measurement gives a potential at one probe only under the assumption that the reference probe is not affected by any correlated the local changes in the potential.

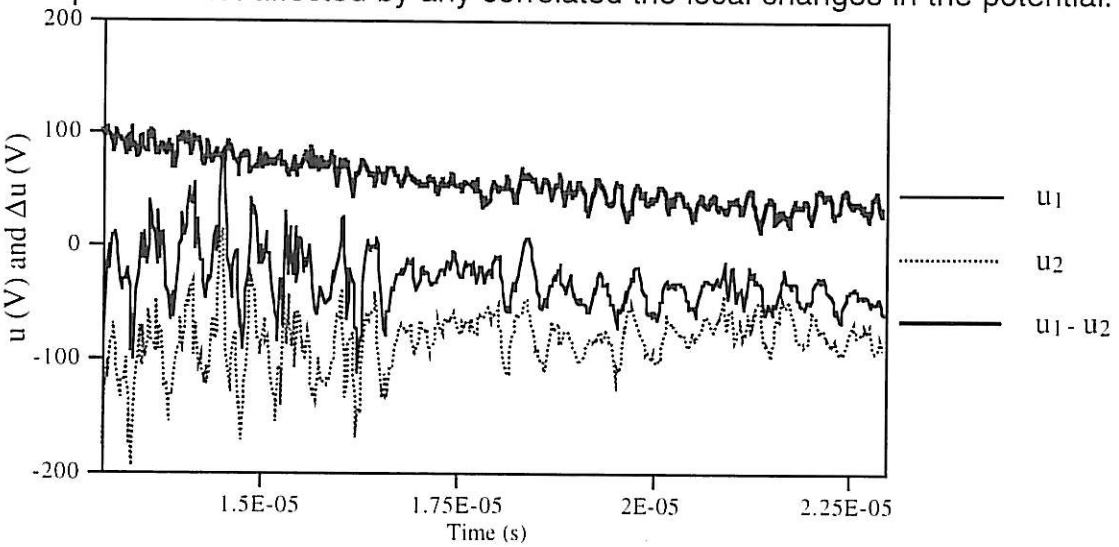

Fig. 25 The potentials u_1 and u_2 and the difference $u_1 - u_2$.

The polarisation electric field

The first part of the plasma pulse arrives at the interaction space 10.5 μs after the main discharge, simultaneously the electric field rapidly increases to the maximum level of approximately 8 kV/m in 0.5 μs (**Fig. 26**). The electric field then decreases, generally faster than the calculated expected electric field (**E**= -**v** x **B**), where v=l/t is obtained from the time after the shot and the distance from the source. Even though there are shot to shot variations, the difference in the rate of decrease is maintained when averaged over 5 shots (**appendix B**). The fact that the measured field is stronger than the calculated for the positive polarised side of the plasma beam is however a known effect (Brenning, Lindberg and Eriksson, 81).

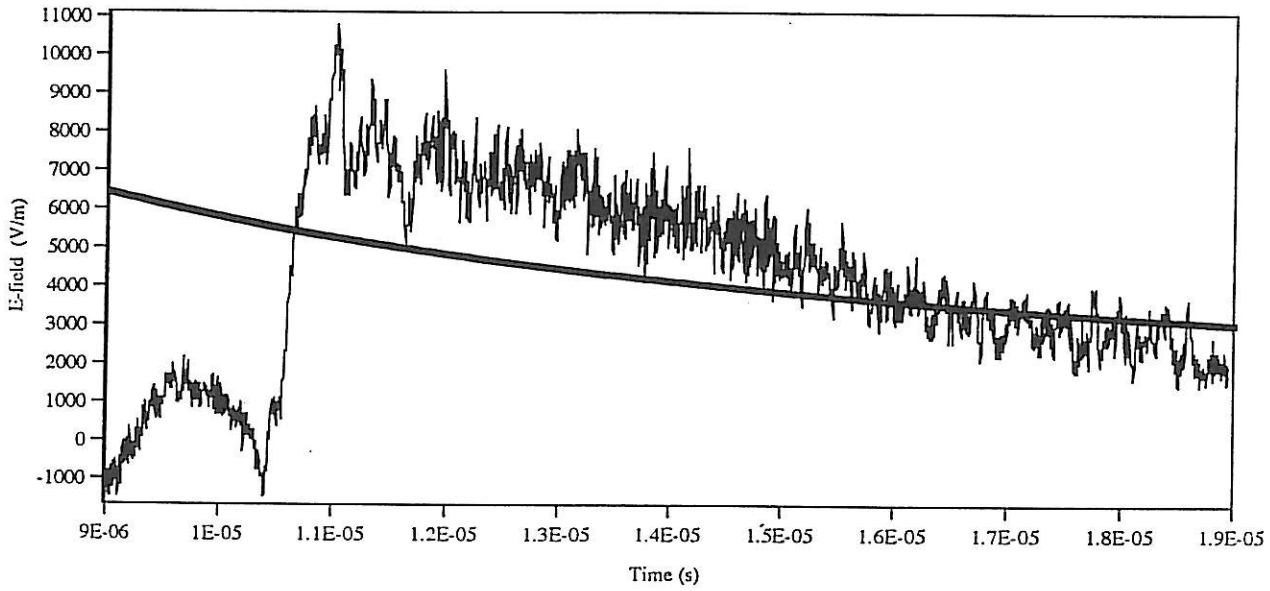

Fig.26 Measured and expected (**E**= -**v** x **B**) electric field from a single shot.

The fluctuating electric field

With the probe configuration of these measurements the fluctuations of the electric field seem to cover a broad band of frequencies. The frequencies of our concern, as discussed in section **3.1**, is above the lower hybrid frequency of 13 MHz. A power spectrum is shown in **Fig. 27b**. The amplitude of the fluctuations are, from **Fig. 26** of the order of 1 kV/m. For a probe separation of 20 mm, 1 kV/m corresponds to a potential difference of 20 V added to the signal of the planned measurements. Fluctuations of about 10 MHz frequencies will compete with the current drop (20 ns). In **Fig. 27a** and **b** the potential difference and the power spectrum of the potential difference are mapped for 5 μs of a shot (t=0 at 13.5 μs after main discharge).

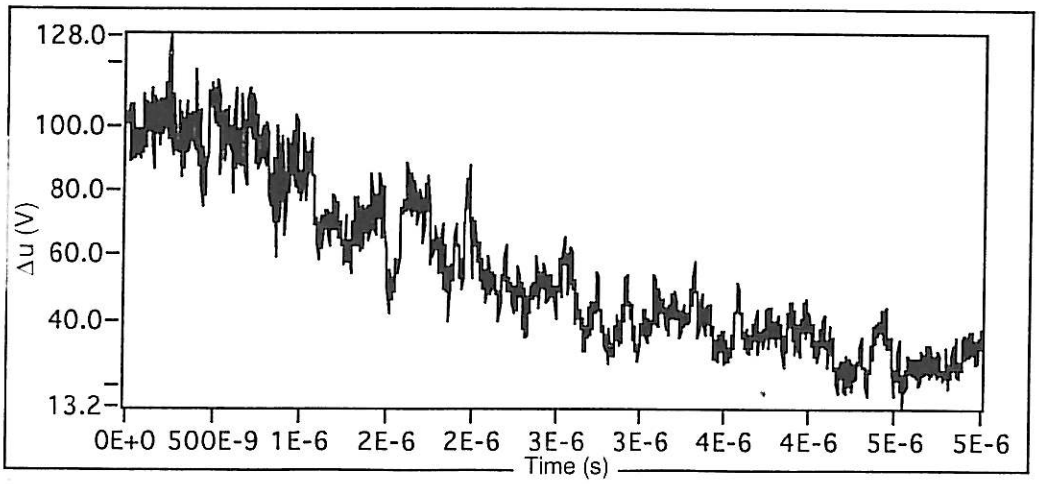

Fig. 27a The potential difference of u_1 and u_2 below the spheres of the disruption probes.

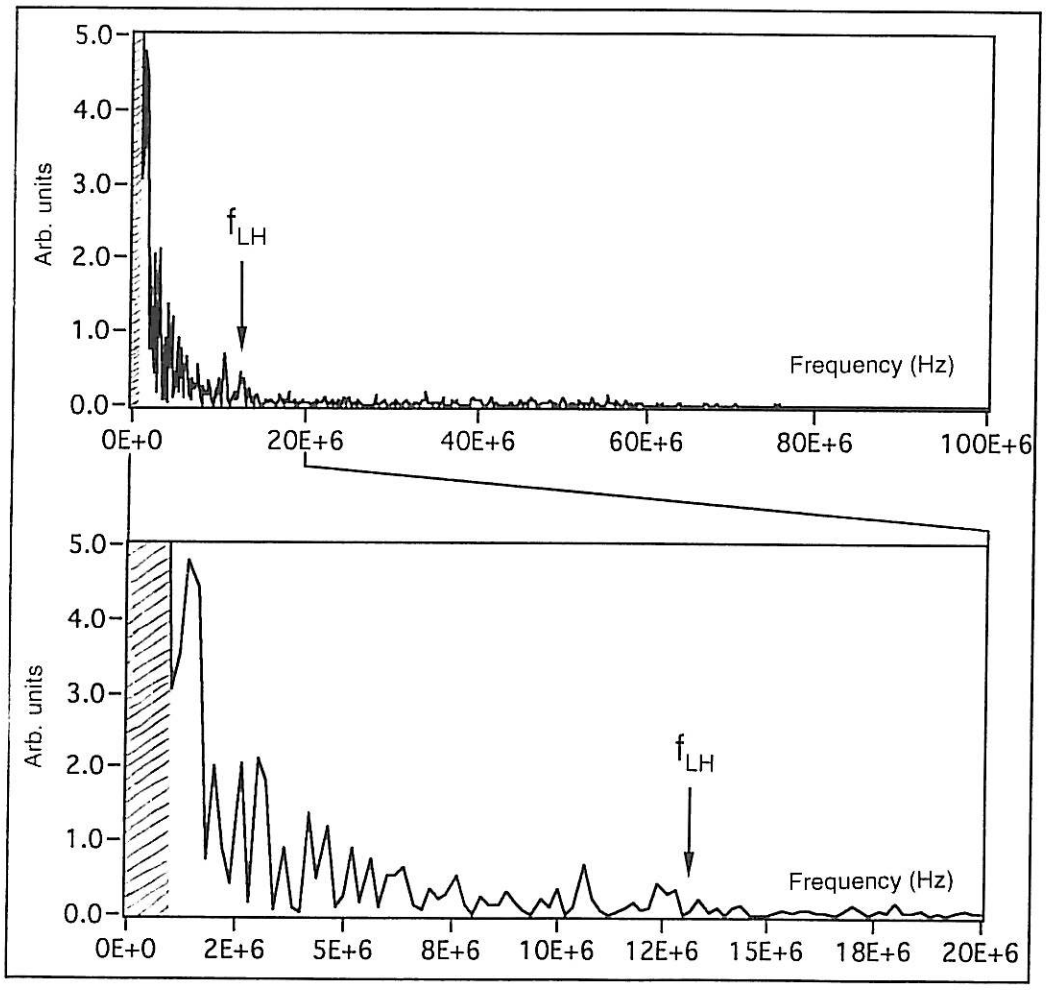

Fig. 27b The power spectrum of the potential difference of u_1 and u_2 below the spheres of the disruption probes. The data is shaded below the frequency corresponding to the sampling interval, where the interpretation is uncertain.

3.4 Density variations in the stream

The current from the density probes (the same probes as used by Svensson, 96) is shown in **Fig. 28a**. The density measurements have been used to check the shot to shot variations. It is known that probes indicate a density approximately twice the density measured with a interferometer (Romedahl, 96 and Lindberg and Kristoferson, 69). In **Fig. 28a** and **b** the density and the power spectrum of the density are shown. Note the strong components between 15 and 45 MHz. The lower hybrid frequency has been calculated to 13 MHz, the lower limit for exiting whistler waves (Stenzel and Urrutia, 90).

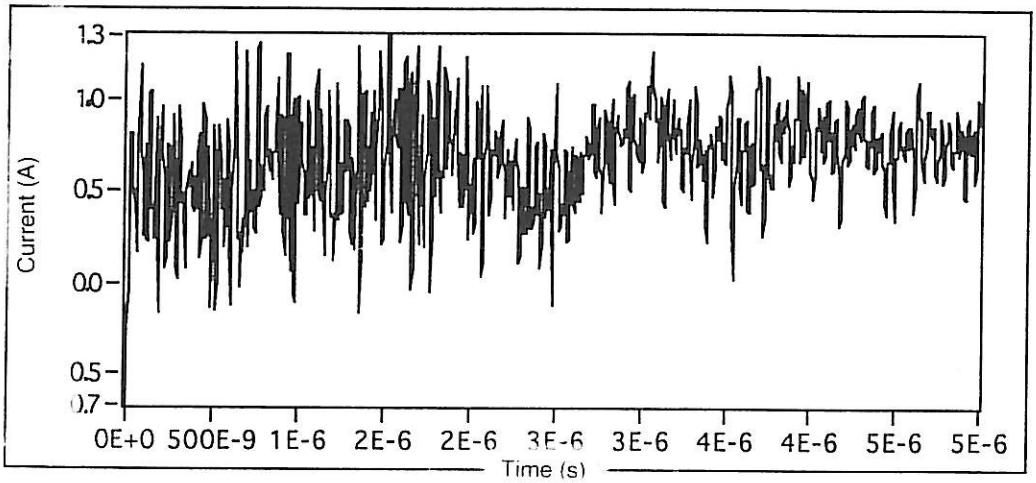

Fig. 28a The current from the density probe.

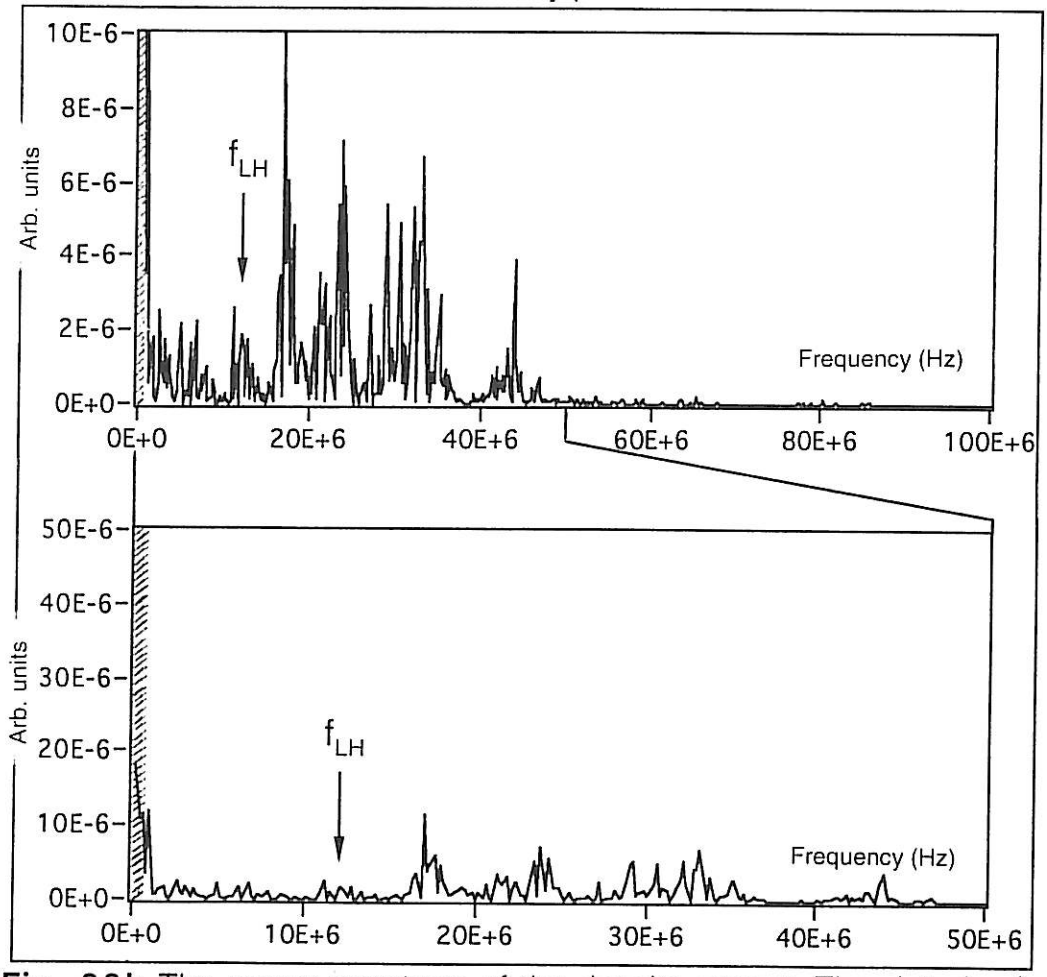

Fig. 28b The power spectrum of the density current. The data is shaded below the frequency corresponding to the sampling interval, where the interpretation is uncertain.

Physics of oscillations in the plasma stream itsef

When the plasma enters the region of the transverse magnetic field, energy is transferred from the ions to the electrons, resulting in heating of the electrons (Brenning, Lindberg and Eriksson, 81). This transition into a transverse magnetic field is also expected to give rise to oscillations in available resonant frequencies. One band of frequencies available for an arbitrary disturbance in the plasma is given by (Stenzel and Urrutia, 90) $\omega_{lh} < \omega < \omega_{ge}$. This corresponds to frequencies ranging from 13 to 560 MHz for our plasma. Oscillations can also arise in other frequency regions. For this plasma the Alfvén band is below 300 kHz, and the electron plasma band is above 180 GHz. The oscillations of special interest is the former that have frequencies of the same order as the disruptions.

3.5 The three observed current cases

The normal mode

For currents limited by either the calculated ion saturation current or the calculated electron saturation current. (Svensson, 96) The current is decided by the incoming flux of ions and electrons to the probes. The geometry of the probes in our experiment gives an electron saturation current, several times the ion saturation current

The high current case

Frequently during the measurements, the current drawn between the disruption probes instead of chopping, rises to a current of 50 A sometimes even more. These currents exceeds the calculated electron saturation current (Svensson, 96). The time for the rise is about 14 μs after main discharge. This is at the same time as the disruptions, if it is a disruptive case, are becoming well defined. The duration of this high current region ranges from 6 to 7 μs, and ends smothly without any sign of disruptive behaviour. At the time of decrease neither the electric field nor the integrated density measured with an interferometer (Romedahl, 96) are undergoing any particular changes. It seems though, that the decrease of the current is acompanied by a decrease in the flux density measured close to the ICP with a directional sensitive density probes. This indicates a correlation between the flux density and the current drawn between the disruption probes.

The disruptive case

The current rises to a level below and close to the electron saturation current and disrupts to a level close to ion saturation current. It is at those rapid disruptions, the changes of the potentials in the vicinity of the ICP will be mapped.

3.6 Potential measurements at the disruptions

The oscillations in the plasma stream itself, described in the previous text, present a problem in measuring the potential effects in the plasma, of a disruption of the current in the plasma driven probe circuit. The common mode fluctuations can be dealt with by differential measurements instead of measurements relative an external ground. However fluctuations of the differential signal are still present, since the reference probe is not stable in potential. The frequencies of these fluctuations correspond to times of the same order as times of the disruptions, and filtering is therefore not possible. To suppress any background fluctuations not correlated to the disruptions. Averages of several disruptions will be made. This reduces changes in the potential difference which are not correlated to the disruption.

Potentials close to the disruption probes

The probe configuration is the same as shown in **Fig. 2 4**. A potential probe is placed 10 mm below the ICP and ECP respectively, and the difference is measured. The disruptions are chosen from the current data alone, without looking at the potential measurements. Examples of disruptions among those not chosen could be those which are very small or disruptions that seems to "hesitate", having a disturbed negative slope (**Fig. 29a**). The amplitudes of the selected disruptions are mainly in the range 1-4 A.

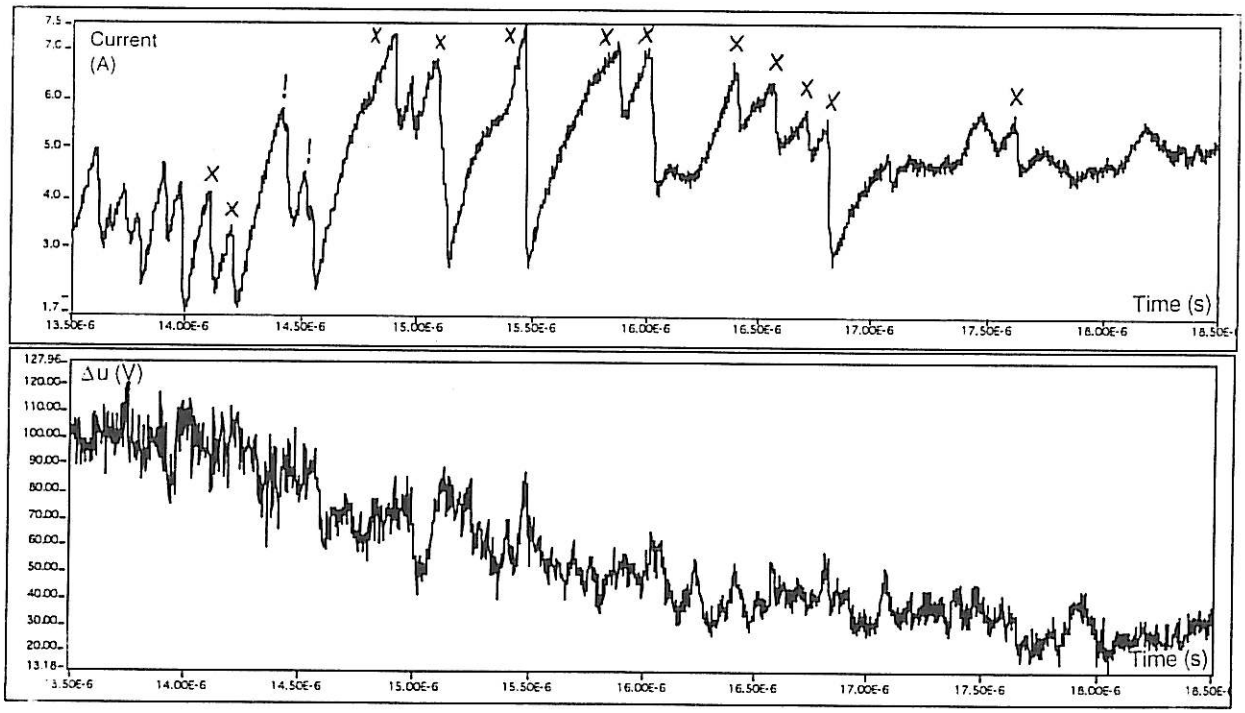

Fig. 29a One of the five shots used for the average contributing with 12 disruptions. Upper curve shows the current of the disruption probes. Disruptions included in the average are marked (**x**), and examples of excluded disruptions are marked (**!**).The lower curve shows the potential difference (u_1-u_2).

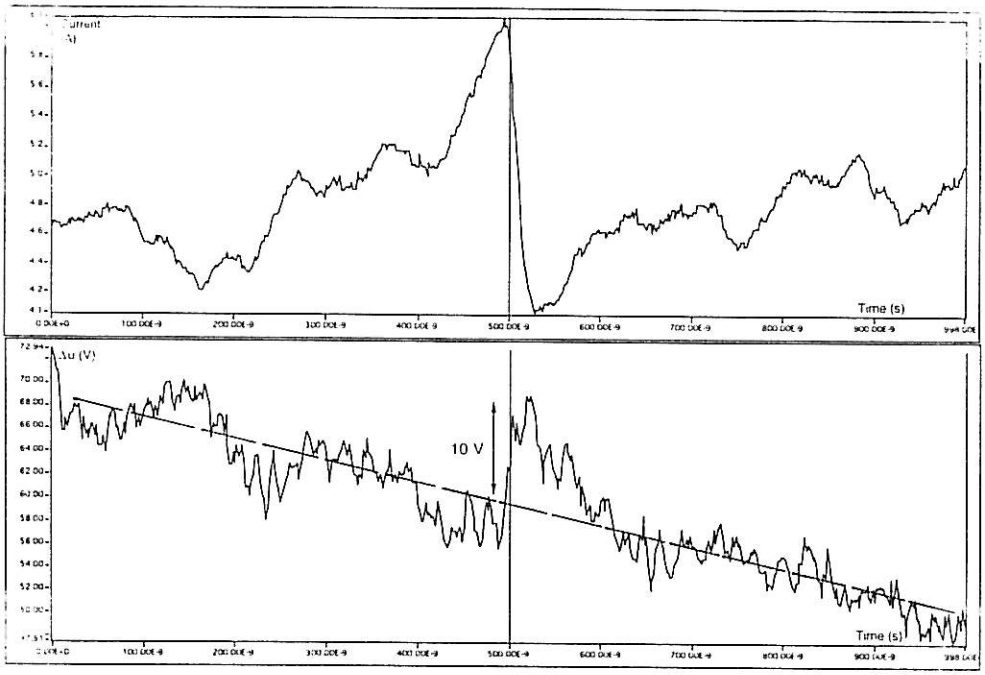

Fig. 29b The upper curve shows the average of the current from the 12 disruptions shown in **Fig. 29a**. The lower curve shows the average of the potential difference (u_1-u_2). The dashed line is an attempt to draw a zero level of the decreasing electric field (**E=-v x B**). It decreases in time due to decreasing velocity of the plasma. There are indications of a 10 v increase in the potential difference during the disruption.

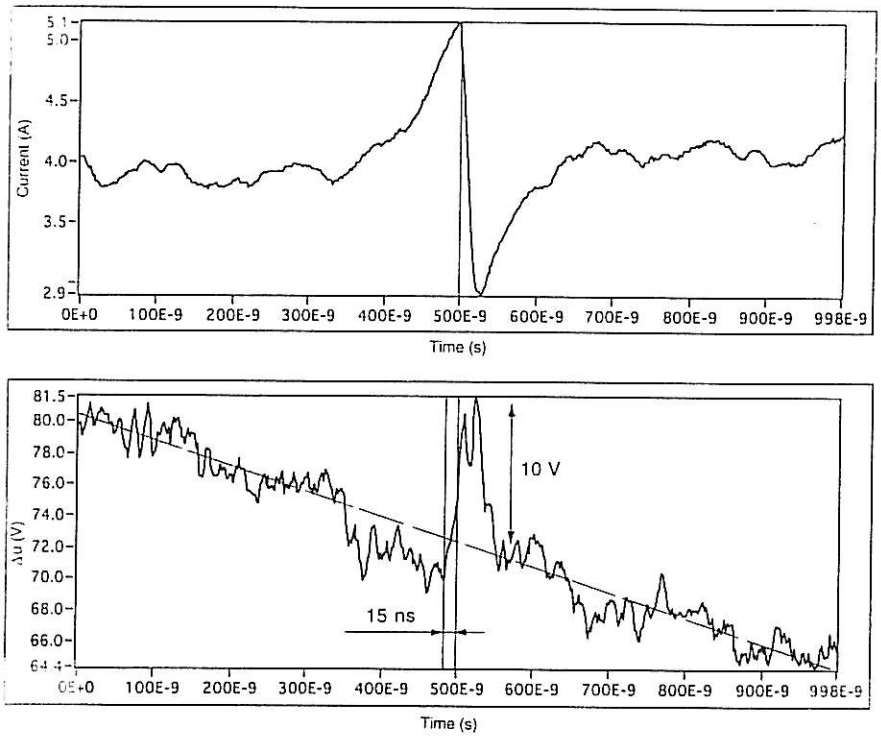

Fig. 29c The upper curve shows the average of the current and the lower curve shows the average of the potential difference (u_1-u_2) of 64 disruptions. The rise of the potential difference at the disruption is even more pronounced for an average of 64 disruptions. The rise seems to precede the disruption by approximately 15 ns.

It seems as if the rise of the potential difference, initiates approximately 15 ns before the current disrupts. In **Fig. 29c** the average is made from 5 shots and a total of 64 selected disruptions. The difference in delay between current and potential measurements, due to different cable lengths is for the cables used of the order of 1 ns which correspond to maximum difference of 20 cm for an estimated signal speed of $2 \cdot 10^8$ m/s. When the current starts to recover, the potential drops simultaneously or later. The fluctuations of the plasma stream itself makes the time of the potential drop uncertain within a period of 10 ns. With the assumption that the potential at the ECP does not change at a disruption (Svensson, 96) the change of the difference in the potentials could be interpreted as a change in the potential of the probe positioned below the ICP. The ICP is known to drop several hundred volts at a disruption due to the induction in the external circuit (Svensson, 96). This measurement shows that the potential close to the ICP rises 10 V at, or possibly slightly before the disruption.
To check if the potential rise at the disruption is statistically significant, an average is made of 5 consecutive time periods of 1 μs from 8 shots, a total of 40 periods. The result of this average is presented in **Fig. 29d**. It is seen that the fluctuations are within ± 2 V of amplitude. The potential rise is thus significant for the disruption.

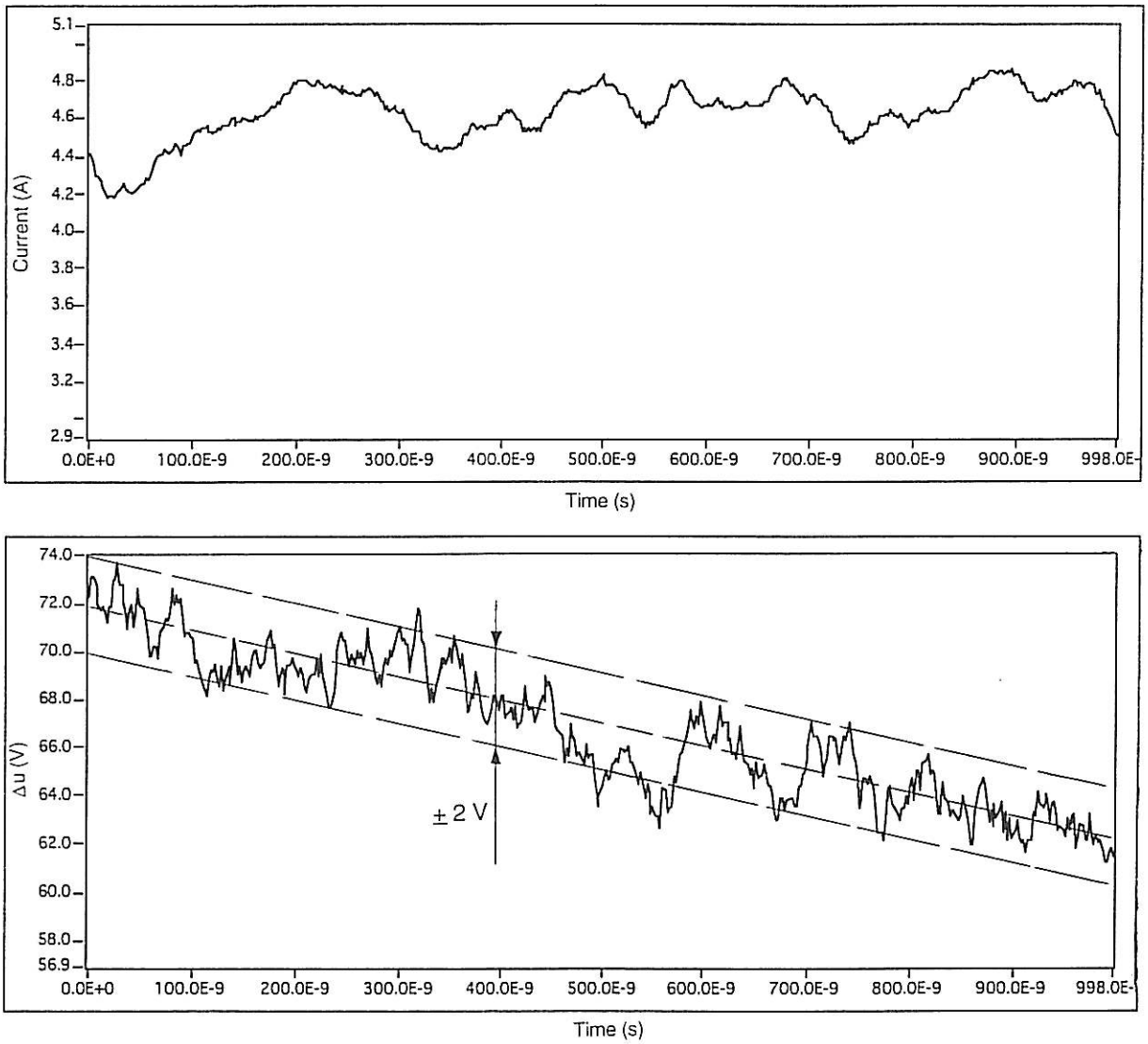

Fig. 29d Average of 40 time periods chosen without correlation to the disruptions.

3.7 Mapping of a plane across B

Potentials at the disruption

The influence of the disruption on the potential difference between two probes at a fixed distance of 10 mm has been investigated at 25 points in a plane 10 mm above the sphere of the ICP. The fluctuating electric field presents a problem in this measurement, just like in the previous. From a single shot it is hard to see a correlation between the potential and the current at the disruption, but when several disruptions are averaged, some tendencies are seen. In **Fig. 30** the potential difference for two interesting positions are presented.

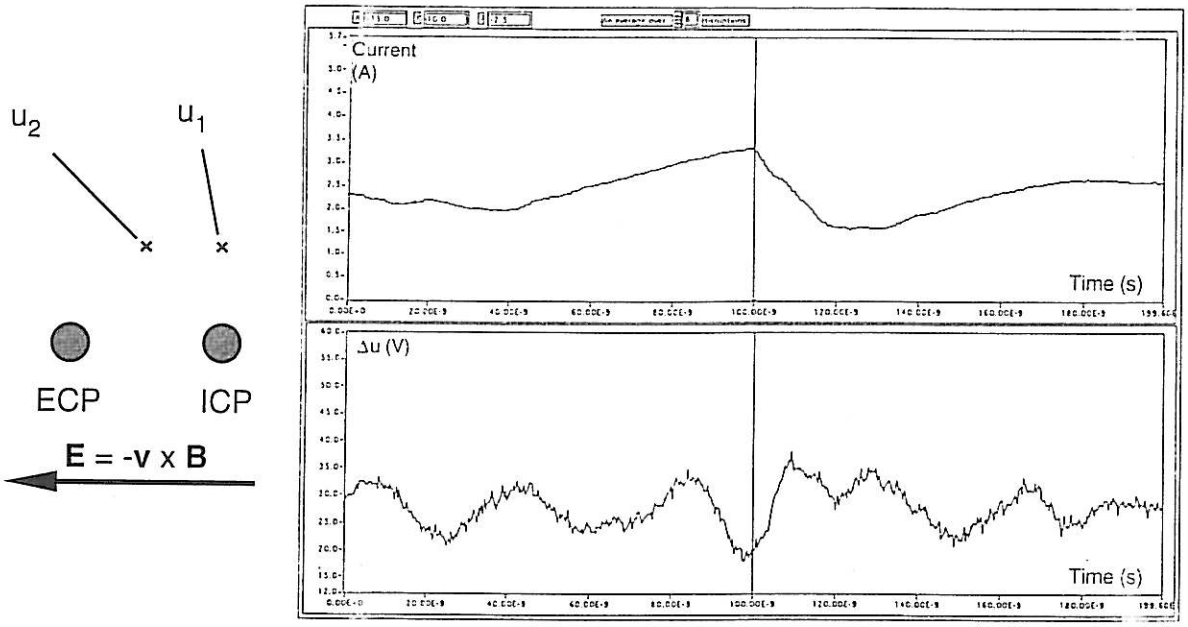

Fig. 30a The probe configuration and the average of 8 disruptions. The upper curve shows the current of the disruption probes and the lower curve shows the potential difference (u_1-u_2).

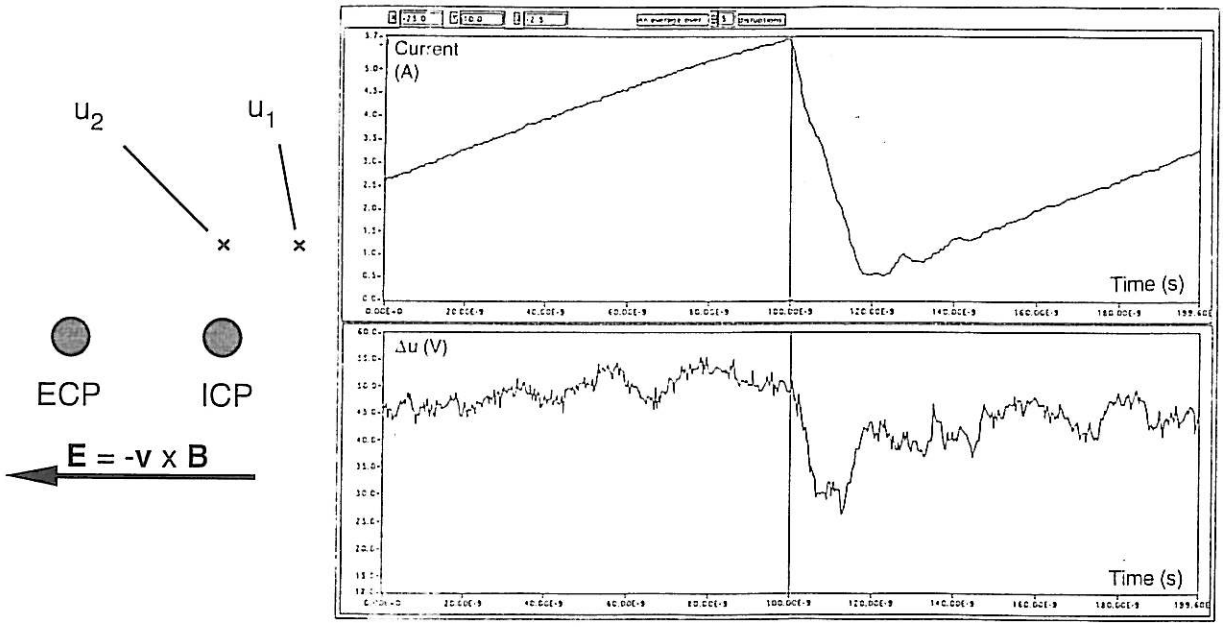

Fig. 30b The probe configuration and the average of 5 disruptions. The upper curve shows the current of the disruption probes and the lower curve shows the potential difference (u_1-u_2).

Since the two potential probes are both close to the ICP, it is not likely that any of the probes is unaffected by changes in potential of the ICP. Therefore the interpretation of the changes in potentials, is restricted to local changes for the actual positions of the potential probes.

In **Fig. 30a** the disruption is accompanied by a rise of the potential probe (u_1) relative the potential probe (u_2) of 20 V, if it is not taken into the account that the potential seems to be at a minimum of an oscillation when the disruption initiates. Otherwise the rise is of the order of 10 V. For the case when the potential probe (u_2) is positioned over the ICP (**Fig. 30b**), the change in potential (u_1-u_2) at the disruption is negative, with the interpretation that the potential above the ICP went more positive at the disruption than the potential 10 mm in the negative X-direction. The rise of the potential is for this position only 5V. It is also noted that the current jump of the disruptions forming this average is half of the amplitude of the disruptions in **Fig. 30a**. This is an inconvenience when it comes to comparing the cases, since the relation between the disruption and potential changes in the vicinity of the spheres are the subject of investigation. However, assuming that the significant potential jumps are all proportional to the current jumps, a consistent picture emerges which for **Fig. 31** is normalised to to a current drop of 2 A in the current. The sphere of the ICP becomes a few hundred volts negative during the disruption (Svensson, 96), while the plasma in the same flux tube at a distance of 10 mm becomes 10 V positive. A qualitative sketch of the situation is shown in **Fig. 31**.

This is consistent with the hypothesis (Svensson, 96) that the current drop is due to a failure of a cathode spot at the ICP. The inductance in the circuit then increases the potential difference over the point where the circuit is broken.

There seems in **Fig. 30a** and **b** to be a small delay of a few ns, from the initiation of the disruption to the rise of the potential. Differences in the cables parameters are not responsible for more than 1 ns. Howerver the fact that the rise of the potential in the measurements presented in **Fig. 29b** and **c** in the previous section preceded the disruption indicates that no certain conclusions about time delays can be made from the present data. Additional examples of averages of the potential difference at different positions above the ICP can be viewed in **appendix C**.

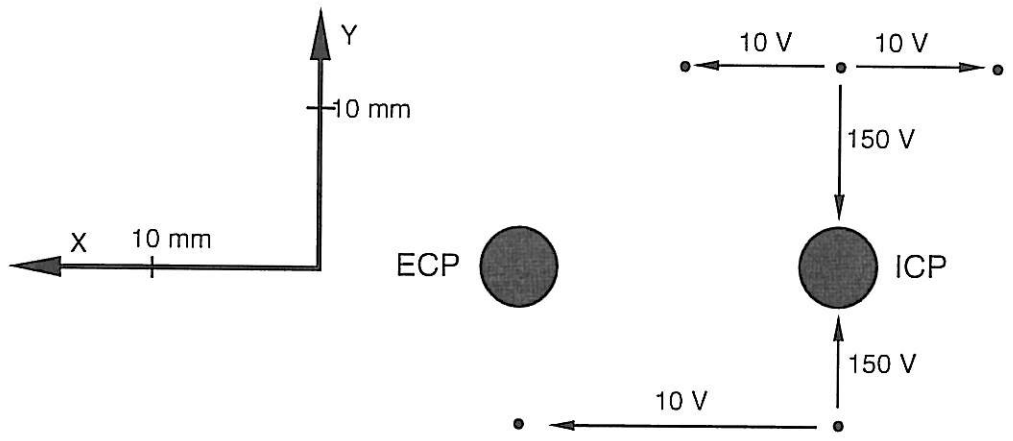

Fig. 31 Local potential differences during the disruption in the rest frame of the plasma, i.e, with the background field **E**= **v** x **B** subtracted. The arrows are pointing to the lower potential.

Density at the disruption

A measurement has been made, similar to the previous potential measurement in a plane above the ICP.The correlation between density variations and current disruptions has been investigated. For none of the positions at which the measurement were performed, an obvious relation between the density and the disruption could be seen by investigation of a single shot. Like in the measurements of the potentials, averages were formed from 10 disruptions at each position. Among the large amplitude oscillations of the density current, no conclusion about an eventual correlation can be made.

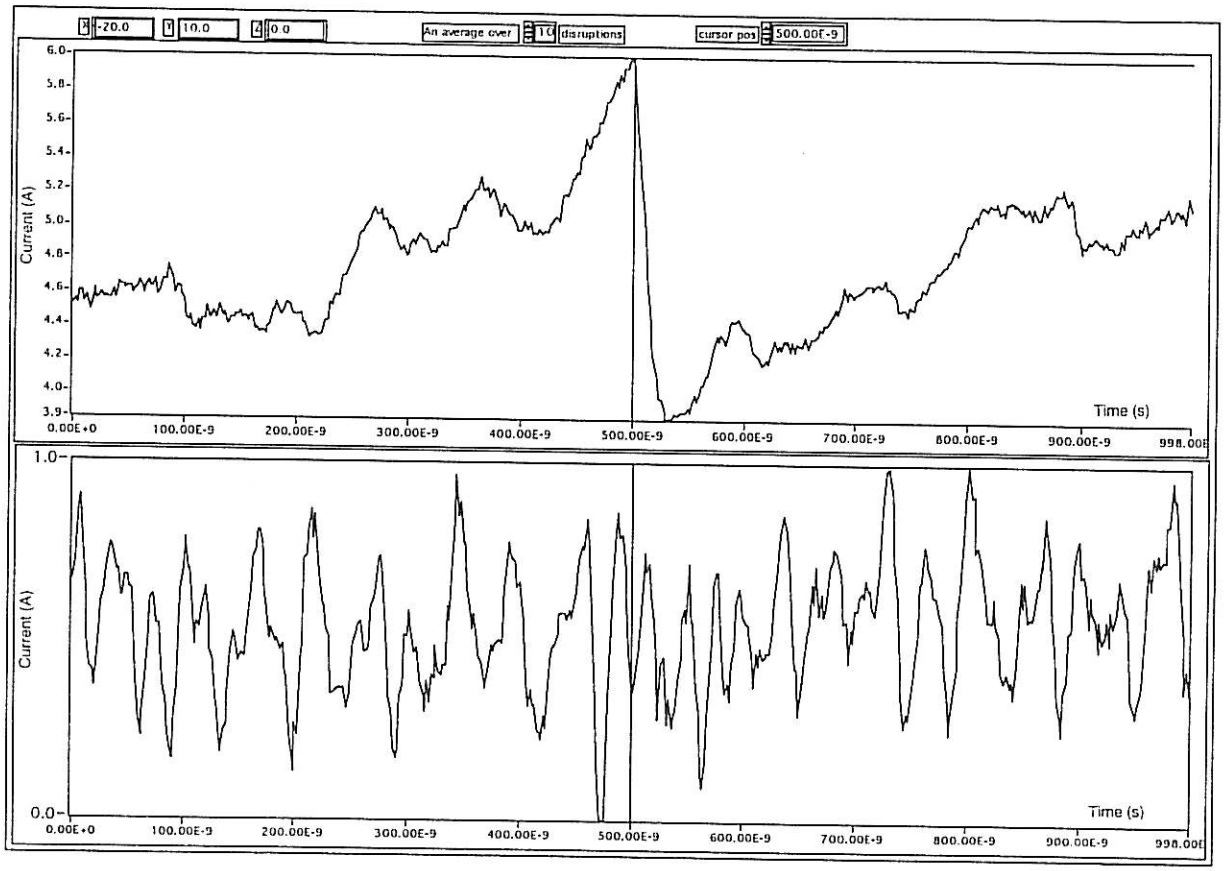

Fig. 3 2 The upper curve shows the current in the circuit of the disruption probes and the lower curve shows the current from the density probe positioned 10 mm above the ICP.

4 Summary and discussion

The rise of the potential in the plasma, close to the ion collecting probe at a disruption in the current in the circuit of the disruption probes encloses the origin of the disruption within 10 mm from the sphere of the ICP, in consistence with the cathode spot theory (Svensson, 96).

The similarities in parameters as described in section **3.1** between this experiment and the synthesised experiment by Stenzel and Urrutia, (90), predicts formation of whistler wings at the spheres of the disruption probes, and currents carried by a wave instead of by particle migration.

The absence of well defined disruptions after the insertion of a Rogowski coil in the vicinity of the disruption probes indicates that the disruptive behaviour is disturbed by the Rogowski coil, but could also be coincidental. Additional measurements could possibly tell if the absence of disruptions is significant for the position of the Rogowski coil, or not.

Acknowledgements

I want to thank my tutor Nils Brenning for tremendous support and secure guidance through this work. I also want to thank Jan Wistedt for a lot of valuable help, and useful instructions in the use of the equipment of the laboratory.

References

Brenning N., Lindberg L. and Eriksson A.
"Energization of electrons in a plasma beam entering a curved magnetic field"
Plasma Physics, Vol. 23, No. 6, 559-574, 1981.

Fälthammar C.- G.
"Plasma fysik" Alfvén laboratory, KTH, Stockholm, Sweden, 1991

Hutchinson I. H.
"Principles of plasma diagnostics" Cambridge University Press, 1987

Lindberg L. and Kristoferson L.
"Electric probe measurements in a moving magnetized plasma"
Report 69-16 Alfvén laboratory (former division of electron and plasma physics), KTH, Stockholm,Sweden, 1969.

Romedahl B.
"Current disruptions in a plasma gun I"
Diploma work thesis at the Alfvén laboratory, KTH, Stockholm, Sweden, 1996.

Stenzel R. L. and Urrutia J. M.
"Currents Between Tethered Electrodes in a Magnetized Laboratory Plasma"
J. Geophys. Res. Vol. 95 No. A5, 6209-6226, 1990

Svensson A.
"Current Disruption in a Plasma Driven Probe Circuit"
Diploma work thesis at the Alfvén laboratory, KTH, Stockholm, Sweden, 1996.

Appendix A

EXT **X-START**
Startpoint of the x-movement relative to an origin chosen

EXT **X-END**
Endpoint of the x-movement relative to an origin chosen

I32 **NUMBER OF STEPS IN X**

EXT **Y-START**
Startpoint of the y-movement relative to an origin chosen

EXT **Y-END**
Endpoint of the y-movement relative to an origin chosen

I32 **NUMBER OF STEPS IN Y**

EXT **Z-START**
Startpoint of the z-movement relative to an origin chosen.

EXT **Z-END**
Endpoint of the z-movement relative to an origin chosen

I32 **NUMBER OF STEPS IN Z**

TF **Speed**
If the LED is lit it is advisable to decrease the output voltage to this motor

TF **Speed**
If the LED is lit it is advisable to decrease the output voltage to this motor

TF **Speed**
If the LED is lit it is advisable to decrease the output voltage to this motor

DBL **Z-step**
This is simply a display of which step of the movement that is currently performed.

DBL **Y-step**
This is simply a display of which step of the movement that is currently performed.

DBL **X-step**
This is simply a display of which step of the movement that is currently performed.

DBL **Length of probe at init in mm**
This lenght is measured manually when the origin has been chosen, and the Z-set off voltage is measured.

TF Pauses the Probe mover program.

DBL **X-setoff Manually**
The set off values of X and Y have to be 1.165 and 1.650 respectively to make the Z-movement parallel to the Z-axis.

DBL **Y-setoff Manually**
The set off values of X and Y have to be 1.165 and 1.650 respectively to make the Z-movement parallel to the Z-axis.

DBL **Z-setoff Manually**
This voltage is measured manually when the probe is at the origin chosen.

TF **measurement**
If no, the program steps through the chosen volume without measuring

DBL **delay**
This should be the total delay you are using

TF **Name files**
In auto mode the coordinates are used as name of the files. Otherwise the program prompts for a file name.

Fig. A1 Explanations of the panel of the LabVIEW program

Appendix B

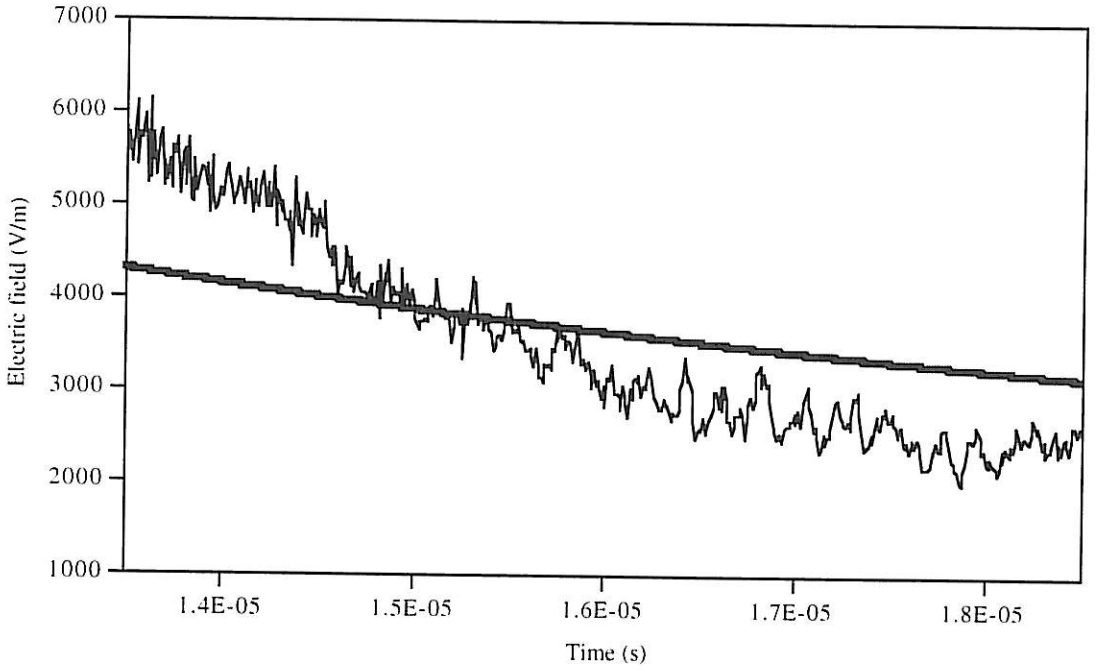

Fig. A2 This diagram shows the average of the electric field from 5 shots. One probe is positioned at the centre of the interaction space and the other probe is positioned 2 cm in the negative X-direction (The positive polarised side). The solid line shows the calculated electric field (**E**=**v** x **B**).

Appendix C

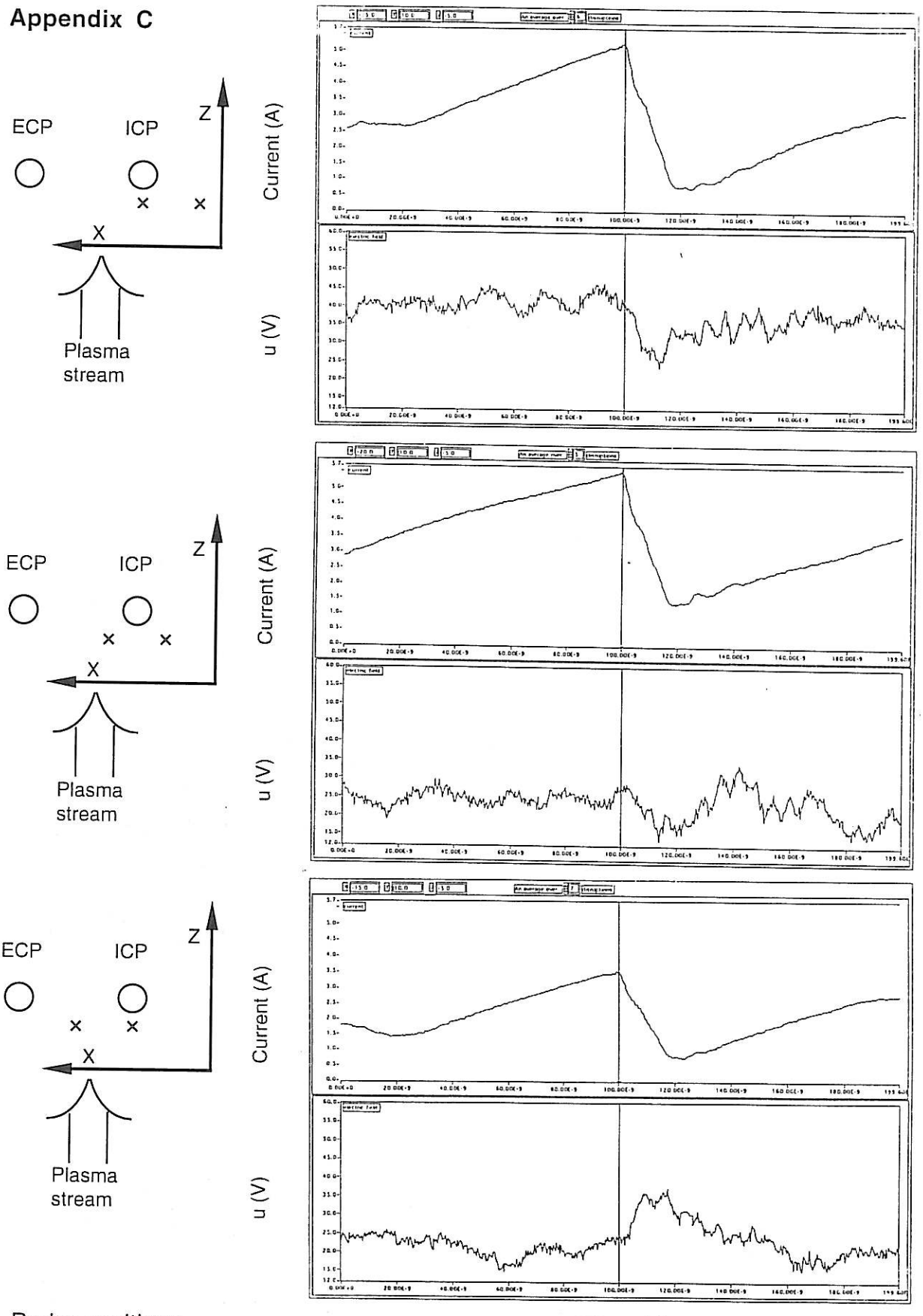

Fig. A3 The positions of the potential probes in a plane 10 mm above the ICP.

Appendix C

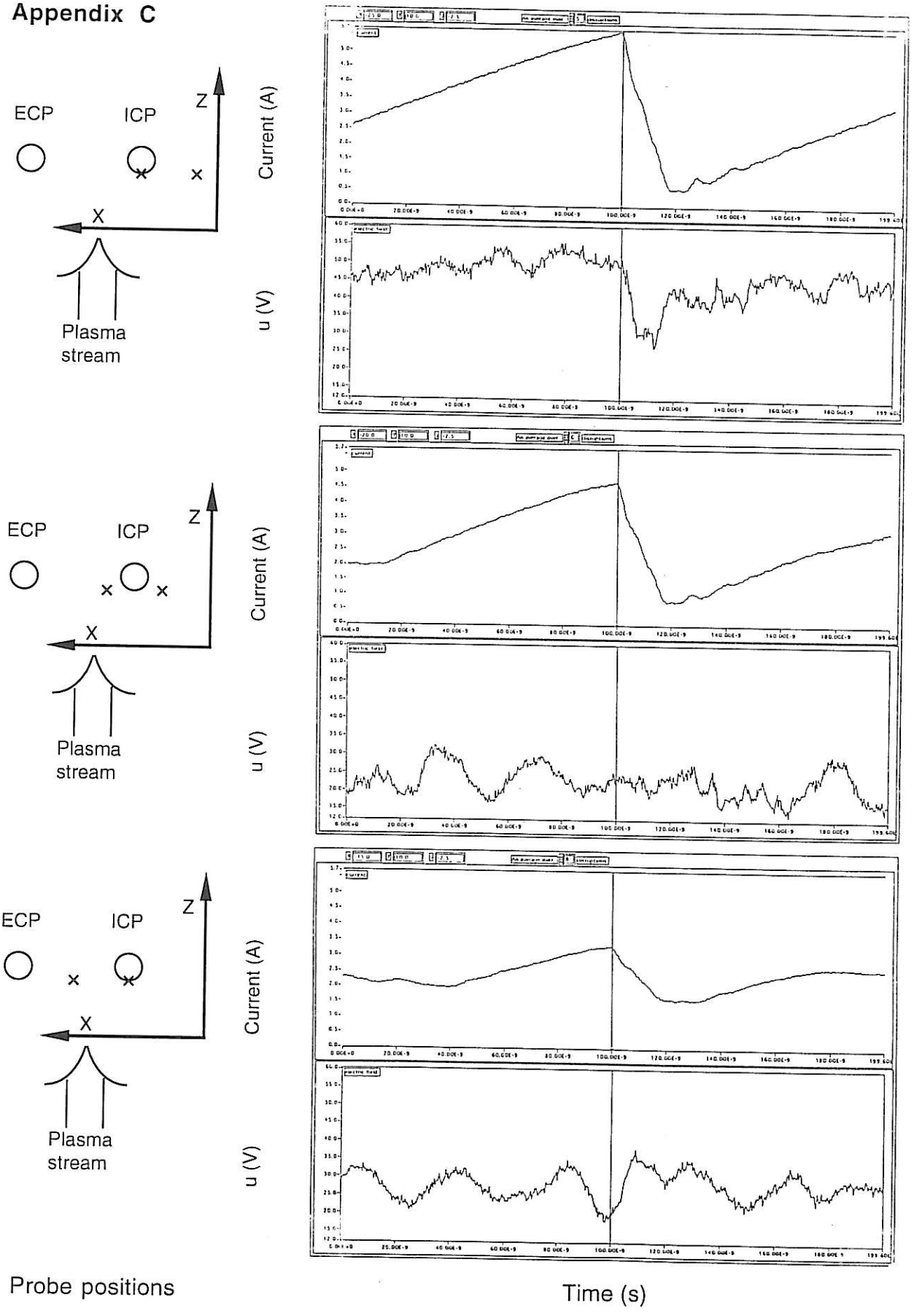

Fig. A4 The positions of the potential probes in a plane 10 mm above the ICP.

Appendix C

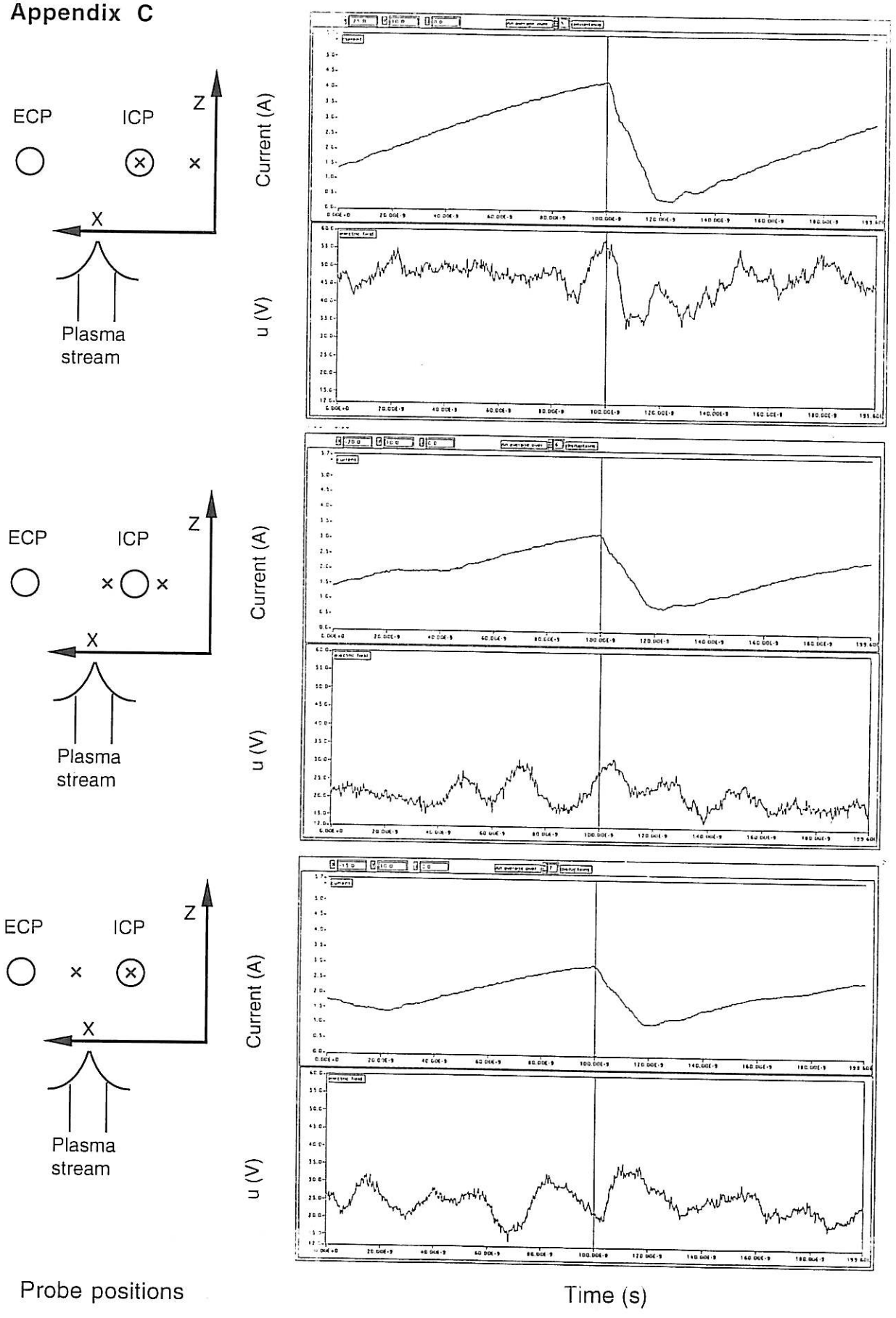

Fig. A5 The positions of the potential probes in a plane 10 mm above the ICP.

Appendix C

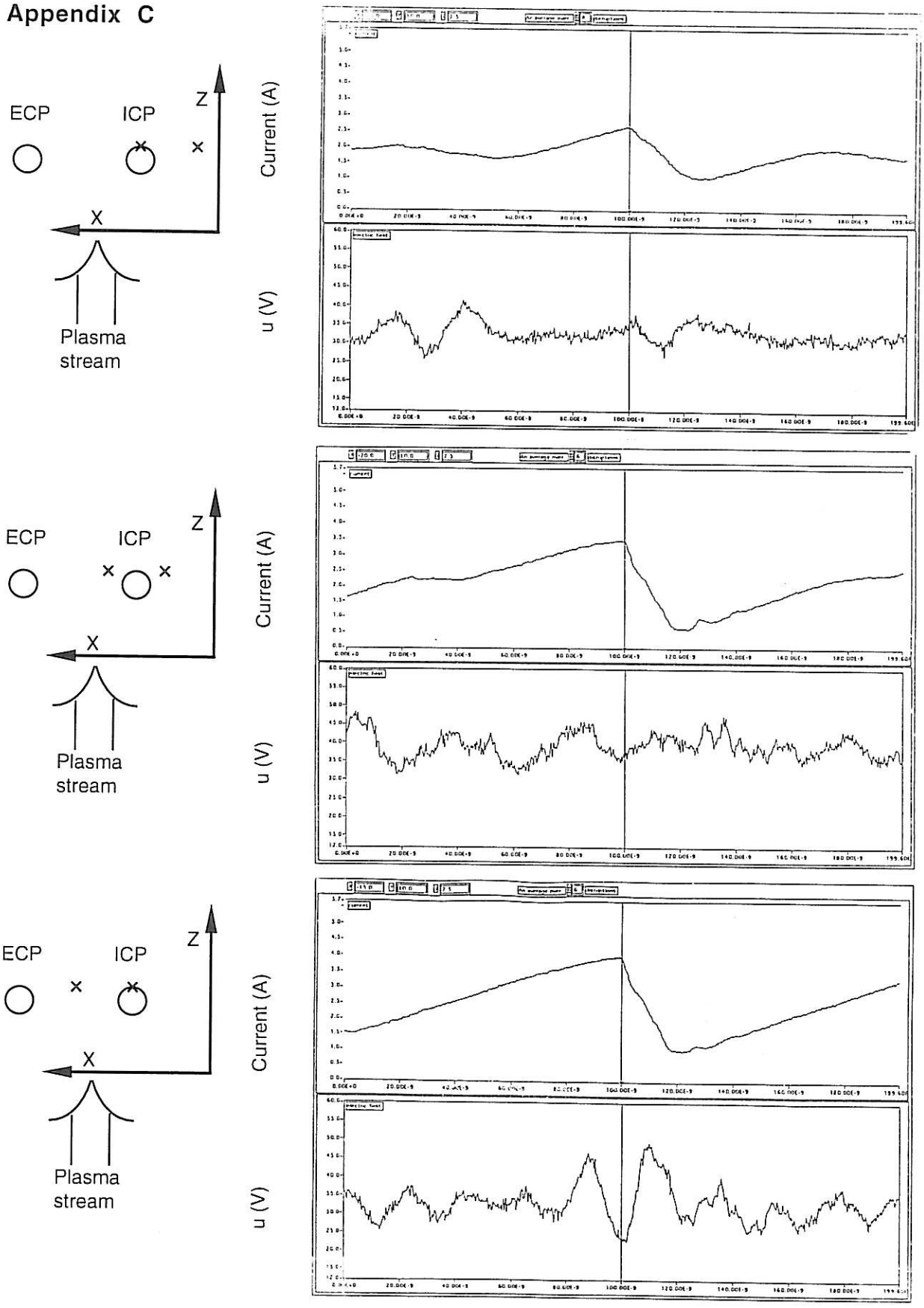

Fig. A6 The positions of the potential probes in a plane 10 mm above the ICP.